Title

Structural Diversity and Magnetic Properties of Hybrid Ruthenium Halide Perovskites and Related Compounds

Journal

Angewandte Chemie International Edition, 59(23)

ISSN

1433-7851 1521-3773

Authors

Vishnoi, Pratap
Zuo, Julia L
Strom, T. Amanda
et al.

Publication Date

2020-04-28

DOI

10.1002/anie.202003095

Peer reviewed

RESEARCH ARTICLE

Structural Diversity and Magnetic Properties of Hybrid Ruthenium Halide Perovskites and Related Compounds

Pratap Vishnoi,[a] Julia L. Zuo,[b] T. Amanda Strom,[a] Guang Wu,[c] Stephen D. Wilson,[b] Ram Seshadri,[a,b,c] and Anthony K.Cheetham*[a,b,d]*

[a] Dr. P. Vishnoi, Dr. T. A. Strom, Prof. R. Seshadri, Prof. A. K. Cheetham
Materials Research Laboratory, University of California, Santa Barbara, CA 93106, United States.
E-mail: ramseshadri@ucsb.edu, akc30@cam.ac.uk
[b] J. L. Zuo, Prof. S. D. Wilson, Prof. R. Seshadri, Prof. A. K. Cheetham
Materials Department, University of California, Santa Barbara, CA 93106, United States.
[c] Dr. G. Wu, Prof. R. Seshadri
Department of Chemistry and Biochemistry, University of California, Santa Barbara, CA 93106, United States.
[d] Prof. A. K. Cheetham
Department of Materials Science & Engineering, National University of Singapore, Singapore 117576.

Supporting information for this article is given via a link at the end of the document.

Abstract: *There has been a great deal of recent interest in extended compounds containing Ru^{3+} and Ru^{4+} in light of their range of unusual physical properties. Many of these properties are displayed in compounds with the perovskite and related structures. Here we report an array of structurally diverse hybrid ruthenium halide perovskites and related compounds: MA_2RuX_6 (X = Cl or Br), MA_2MRuX_6 (M = Na, K or Ag; X = Cl or Br) and $MA_3Ru_2X_9$ (X = Br) based upon the use of methylammonium ($MA = CH_3NH_3^+$) on the perovskite A site. The compounds MA_2RuX_6 with Ru^{4+} crystallize in the trigonal space group $R\bar{3}m$ and can be described as vacancy-ordered double-perovskites. The ordered compounds MA_2MRuX_6 with M^+ and Ru^{3+} crystallize in a structure related to $BaNiO_3$ with alternating MX_6 and RuX_6 face-shared octahedra forming linear chains in the trigonal $P\bar{3}m$ space group. The compound $MA_3Ru_2Br_9$ crystallizes in the orthorhombic Cmcm space group and displays pairs of face-sharing octahedra forming isolated Ru_2Br_9 moieties with very short Ru-Ru contacts of 2.789 Å. The structural details, including the role of hydrogen bonding and dimensionality, as well as the optical and magnetic properties of these compounds are described. The magnetic behavior of all three classes of compounds is influenced by spin-orbit coupling and their temperature-dependent behavior has been compared with the predictions of the appropriate Kotani models.*

Introduction

Since the discovery of the remarkable optoelectronic properties of Pb-based hybrid perovskite halides such as $MAPbI_3$ ($MA = CH_3NH_3$),[1–4] a great deal of interest has focused on related systems of general formula AMX_3 (*A* = monovalent cation such as CH_3NH_3; *M* = bivalent metal ion such as Pb or Sn; *X* = halide such as Cl, Br or I). On account of the toxicity of Pb, there has also been a significant activity associated with perovskites based on other divalent metals.[5–10] In addition, simultaneous replacement of the divalent ion with a monovalent and a trivalent metal ion gives rise to double perovskites, $A_2MM'X_6$. Owing to the tuneability of *M* and *M'*, the hybrid double perovskites show great chemical diversity. For example, the neighbors of Pb in the periodic table, such as Ag, Sb, Tl, and Bi have been employed for the synthesis of Pb-free hybrid double perovskites, many of which show excellent optoelectronic and other properties.[11–14]

Beyond hybrid double perovskites, the high level of interest in this area has led to significant activity in related perovskite chemistries, including the study of 1-D and layered hybrid structures.[15–22] There is also growing interest in hybrid *M*-site vacancy halide perovskites of general formula A_2MX_6, which are related to the well-known K_2PtCl_6 structure. For example, the discovery of MA_2PtCl_6 and related materials containing Pt(IV) and Sn(IV) has been recently reported.[23–25] MA_2SnI_6 absorbs in the visible and near-infrared regions of the solar spectrum.[25] Hybrid halide perovskites and related compounds, together with their structural relationships, are displayed schematically in Figure 1.

In the present work, we extend the domain of hybrid halide perovskites to the study of ruthenium-containing compounds. There is an extensive literature on ruthenium oxide perovskites such as 3D $ARuO_3$ (*A* = Ca, Sr or Ba) and $A_{n+1}Ru_nO_{3n+1}$ (*A* = Ca, Sr or Ba; *n* = 1, 2 or 3) type Ruddlesden-Popper structures. These oxides show a wide range of exciting properties, such as proposed spin-triplet superconductivity in Sr_2RuO_4[26,27] and the coexistence of ferromagnetism and metallic conductivity in $SrRuO_3$.[28–30] More recently, many Ru compounds have been studied in light of the interplay between spin-orbit coupling and electron correlation.[31] In particular, α-$RuCl_3$ has been suggested[32] potentially host a Kitaev quantum spin liquid ground state[33] which may be relevant for quantum computing. New chemistry on this layered compound has been emerging apace.[34,35] There are a small number of inorganic ruthenium halides with perovskite-related structures such as K_2RuCl_6,[36,37] but very few hybrid halides of Ru have been reported.[38,39] The magnetic properties of some of these compounds have been investigated[38] and their temperature-dependent magnetic moments are found be broadly in accord with the Kotani theory.[40,41]

We describe here the discovery and characterization of nine methylammonium Ru halides belonging to three families: $MA_2Ru^{IV}X_6$ (*X* = Cl or Br), **1** and **2**; $MA_2MRu^{III}X_6$ (*M* = Na, K or Ag;

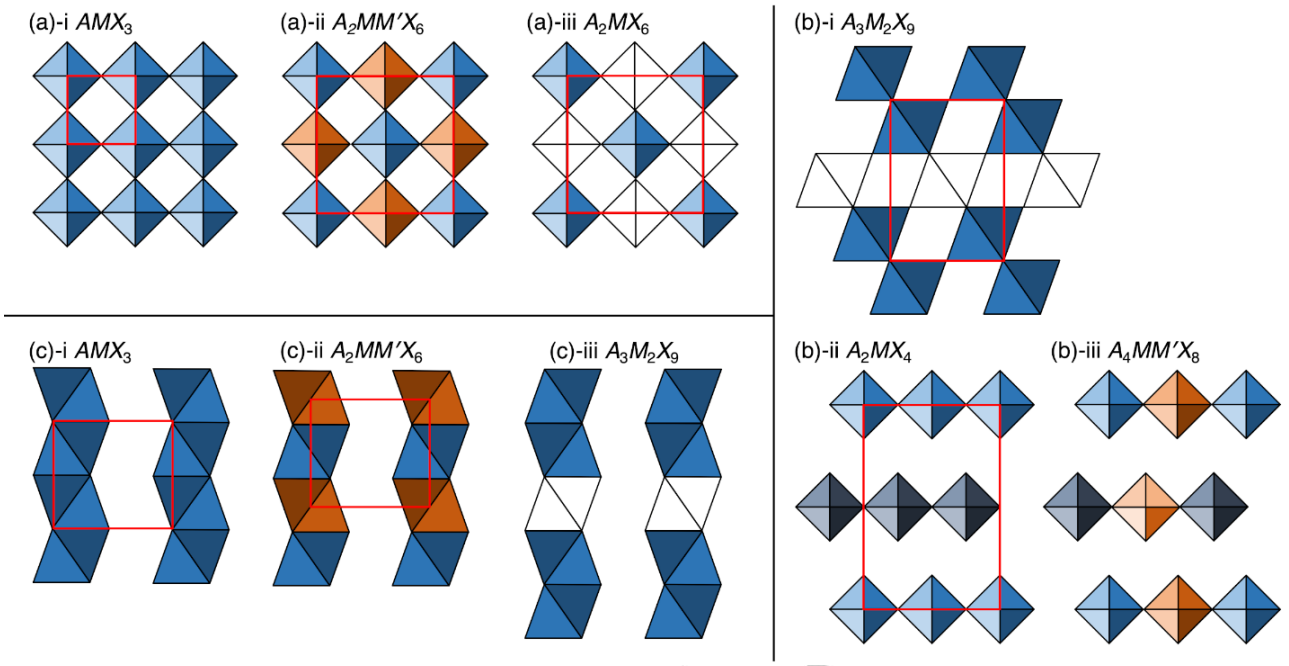

Figure 1. Schemes displaying the relationships between idealized perovskite-derived structures and related compounds. For clarity, the *A* moieties are not displayed. (a)-i: The AMX_3 perovskite aristotype. (a)-ii: The ordered double perovskite structure of $A_2MM'X$. (a)-iii: The vacancy-ordered double perovskite A_2MX_6, with every second *M'* replaced by a vacancy. (b)-i: The layered vacancy-ordered perovskite $A_3M_2X_9$, with every third *M* atom is missing. (b)-ii: The n = 1 Ruddlesden-Popper structure of A_2MX_4. (b)-iii: The ordered ("double") variant of the n = 1 Ruddlesden-Popper compound, $A_4MM'X_8$. (c)-i: The face-sharing octahedral $BaNiO_3$-type structure of AMX_3. (c)-ii: The ordered variant ("double") of the $BaNiO_3$ structure with the formula $A_2MM'X_6$. (c)-iii: The idealized, vacancy ordered faced-shared hexagonal structure deriving from $BaNiO_3$, or $A_3M_2X_9$. The structures types represented in this contribution are (a)-iii, (c)-ii, and (c)-iii.

Table 1. Structural properties of methylammonium Ru Halides **1**-**9**.

Compounds	Crystal symmetry	Unit cell dimensions (Å) and volumes (Å^3)	Structure type[a]
MA_2RuCl_6 (1)	Trigonal, $R\bar{3}m1$ (# 166)	$a = b$ = 6.9935(3); c = 21.9740(12); V = 930.74(9)	(a)-iii A_2MX_6
MA_2RuBr_6 (**2**)	Trigonal, $R\bar{3}m1$ (# 166)	$a = b$ = 7.3485(10); c = 22.376(4); V = 1046.4(3)	(a)-iii A_2MX_6
$MA_2NaRuCl_6$ (**3**)	Trigonal, $P\bar{3}m1$ (# 164)	$a = b$ = 7.2493(9); c = 6.7926(8); V = 309.14(8)	(c)-ii $A_2MM'X_6$
$MA_2AgRuCl_6$ (**4**)	Trigonal, $P\bar{3}m1$ (# 164)	$a = b$ = 7.237(5); c = 6.936(5); V = 314.6(5)	(c)-ii $A_2MM'X_6$
MA_2KRuCl_6 (**5**)	Trigonal, $P\bar{3}m1$ (# 164)	$a = b$ = 7.181(5); c = 7.366(5); V = 329.0(5)	(c)-ii $A_2MM'X_6$
$MA_2NaRuBr_6$ (**6**)	Trigonal, $P\bar{3}m1$ (# 164)	$a = b$ = 7.561(5); c = 7.105(5); V = 351.8(5)	(c)-ii $A_2MM'X_6$
$MA_2AgRuBr_6$ (**7**)	Trigonal, $P\bar{3}m1$ (# 164)	$a = b$ = 7.516(5); c = 7.032(4); V = 344.1(5)	(c)-ii $A_2MM'X_6$
MA_2KRuBr_6 (**8**)	Trigonal, $P\bar{3}m1$ (# 164)	$a = b$ = 7.4892(17); c = 7.3894(18); V = 358.93(18)	(c)-ii $A_2MM'X_6$
$MA_2Ru_2Br_9$ (**9**)	Orthorhombic, *Cmcm* (# 63)	a = 7.3797(16); b = 15.167(4); c = 18.419(5); V = 2061.6(9)	(c)-iii $A_3M_2X_9$

[a] Different structure types are shown in Figure 1.

X = Cl or Br), **3**-**8**; and $MA_3Ru^{III}{}_2X_9$ (*X* = Br), **9**. The crystal structures and the optical and magnetic properties of these compounds have been determined and their behavior is compared with related inorganic compounds that have been described in the literature.

Results and Discussion

$MA_2Ru^{IV}Cl_6$ (**1**), $MA_2Ru^{IV}Br_6$ (**2**), $MA_2NaRu^{III}Cl_6$ (**3**), $MA_2AgRu^{III}Cl_6$ (**4**), $MA_2KRu^{III}Cl_6$ (**5**), $MA_2NaRu^{III}Br_6$ (**6**), $MA_2AgRu^{III}Br_6$ (**7**), $MA_2KRu^{III}Br_6$ (**8**) and $MA_3Ru^{III}{}_2Br_9$ (**9**) have been synthesized solvothermally and their structures have been determined by single-crystal X-ray diffraction (see supporting information for the details). Compounds **1** and **2** were obtained from the reaction of $RuCl_3$ with methylammonium chloride in aqueous HCl and methylammonium bromide in aqueous HBr, respectively. During the reactions in acidic media, Ru^{3+} oxidized to Ru^{4+} and these Ru^{4+} ions were utilized in the formation of **1** and **2**. In the cases of the compounds **3**-**8**, however, where the simultaneous incorporation of M^+ and Ru^{3+} ions is necessary to form the structures, the oxidation of Ru^{3+} needed to be

suppressed. This was achieved by using stoichiometric quantities (one equivalent relative to the $RuCl_3$) of hypophosphorous acid (H_3PO_2). The diruthenium compound, $MA_3Ru_2Br_9$ (**9**), was obtained along with **8** from the reaction of methylammonium bromide, KCl, $RuCl_3$ and H_3PO_2 in HBr. Details of the X-ray data collection and structure refinement are provided in supporting information, Table S1 and selected bond distances are listed in Table S2. Selected bond angles are given in Tables S3-S6 (supporting information).

Compounds **1** and **2** are isostructural and crystallize in the rhombohedral space group, $R\bar{3}m$ (Table 1) as reported previously for the case of MA_2PtI_6.[24] Figure 2 shows the unit cells of **1** and **2**. The compounds contain isolated $[RuX_6]^{2-}$ octahedra together with methylammonium cations in a motif. The structures are very similar to the vacancy-ordered double perovskites such as K_2RuCl_6 with A_2MX_6 as the structure type (Figure 1).[42] Unlike the cubic K_2RuCl_6, however, **1** and **2** lack a 4-fold symmetry axis due to a rhombohedral distortion that is caused by the alignment of the methylammonium cations. The Ru-Cl and Ru-Br bond distances [2.327(1) Å and 2.483(1) Å, respectively] are similar to those in other low-spin d^4 Ru^{4+} halides with octahedral coordination (supporting information, Table S2).[38] The bond angles within the RuX_6 octahedra are extremely close to 90° and 180° (supporting information, Table S3), though this is not required by the crystal symmetry. We ascribe the regularity of the RuX_6 octahedra to the very high ligand field stabilization energy associated with the low spin d^4 configuration of octahedral Ru^{4+}.

The structures of **1** and **2** are stabilized by hydrogen bonding between the halide ligands and methylammonium cations (Figure 3 and supporting information, Figure S1), with the head-to-tail arrangement of methylammonium cations maximizing the N−H···*X* hydrogen bond interactions. The shortest donor-acceptor N···Cl distance in the case of **1** is 3.432 Å which is comparable to those found in systems with NH_3^+ as the donors and Cl^- as the acceptors such as layered Cu(II) perovskites with methylammonium cation (3.402 Å).[43] The shortest N···Br distance in **2** (3.568 Å) is slightly longer than the corresponding distances in related compounds (e.g. 3.440 Å).[44,45]

Compounds **1** and **2** show broad optical absorption spanning almost the entire ultraviolet and visible regions, and these Ru^{4+} compounds appear black. Compound **1** shows two broad absorption bands centered around 4.43 and 2.43 eV (Figure 4) which can be ascribed to ligand to metal charge transfer (LMCT).[46] Due to the strong oxidizing nature of Ru^{4+}, the symmetry allowed charge transfer bands obscure the weak bands arising from *d-d* transitions. The spectrum of **2** is slightly broadened and shifted to the red due to the lower electron affinity of Br compare to Cl. The LMCT absorption bands are positioned around 3.54 and 1.55 eV in the case of **2**. The multiple bands observed below 1.0 eV nm are due to the C-H overtones of the methylammonium cation, which was confirmed by measuring the spectrum of methylammonium chloride (supporting information, Figure S2).

The magnetic susceptibility measurements on **1** enabled us to calculate the effective magnetic moment as a function of temperature for this compound. Due to the isolated and undistorted nature of the $RuCl_6$ octahedra in MA_2RuCl_6 and the intermediate strength of the spin-orbit coupling in Ru^{4+}, at these temperatures we expect these compounds to exhibit single-ion behavior without the influence of exchange interactions as described previously for related materials containing isolated RuX_6^{2-} and RuX_6^{3-} ions.[38] This behavior was first described quantitatively by Kotani for an octahedral crystal field environment and follows a series of universal curves that depend on the *d* electron configuration when plotted against the unitless quantity k_BT/ξ (where ξ is the spin-orbit coupling constant). The theoretical dependencies of m_{eff} versus k_BT/ξ are shown in Figure 5 as solid black lines for low spin d^4 Ru^{4+} and low spin d^5 Ru^{3+} ions. The experimental data for **1** are in excellent agreement with the Kotani plot calculated using a spin-orbit coupling constant ξ of 1400 cm^{-1}. This value is consistent with measurements on other low spin d^4 Ru^{4+} compounds such as $(NH_4)_2RuCl_6$,[38] and K_2RuCl_6.[47] At low temperatures, the effective moment of **1** falls sharply to the ground state $J = 0$. There is no evidence for deviations due to coupling between the widely spaced Ru^{4+} ions.

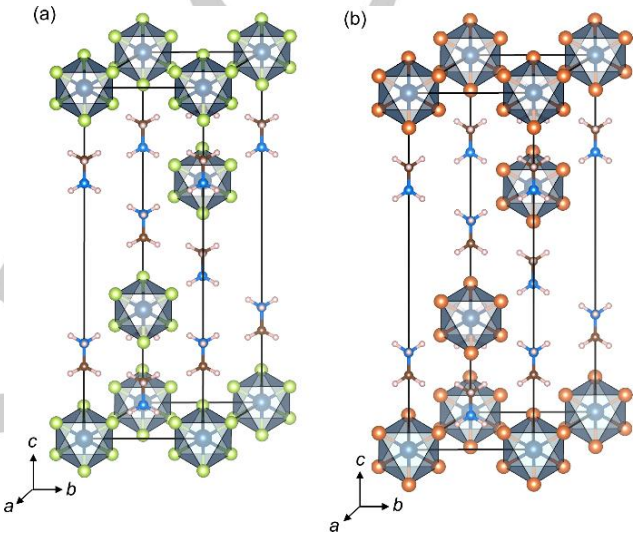

Figure 2. Single-crystal structures (unit cells) of MA_2RuX_6. (a) MA_2RuCl_6 (**1**). (b) MA_2RuBr_6 (**2**). The isolated octahedra show $RuCl_6$ and $RuBr_6$ units. Methylammonium cations are present in the space between the octahedra in a head-to-tail arrangement.

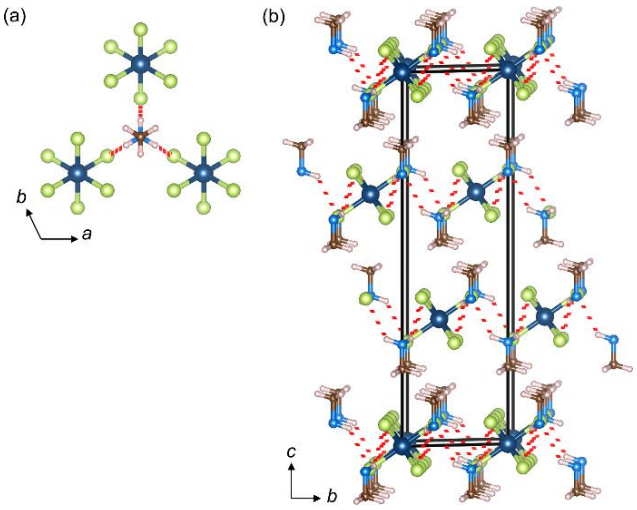

Figure 3. Hydrogen bond interactions in MA_2RuCl_6 (**1**). (a) The ball and stick model of three $RuCl_6$ octahedra connected with a methylammonium cation by hydrogen bonds. The red dotted lines show hydrogen bond interactions. (b) The packing diagram shows layer formation in the *ab*-plane due to the N−H···Cl hydrogen bonds.

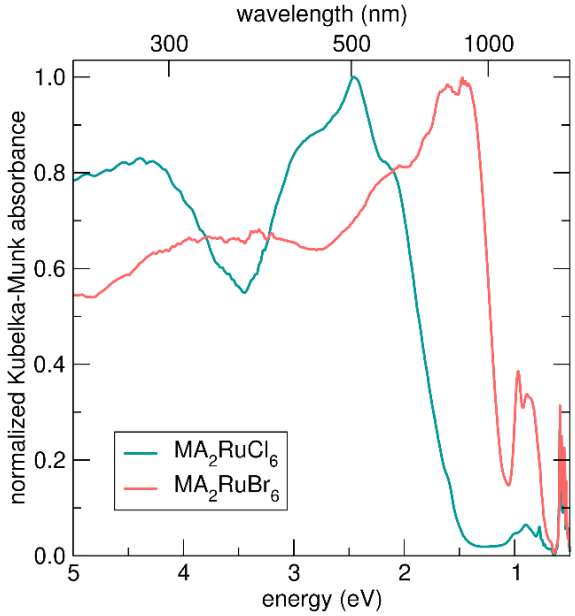

Figure 4. Absorption spectra of MA_2RuCl_6 (**1**) and MA_2RuBr_6 (**2**) obtained from the Kubelka-Munk transformation of the diffuse reflectance data.

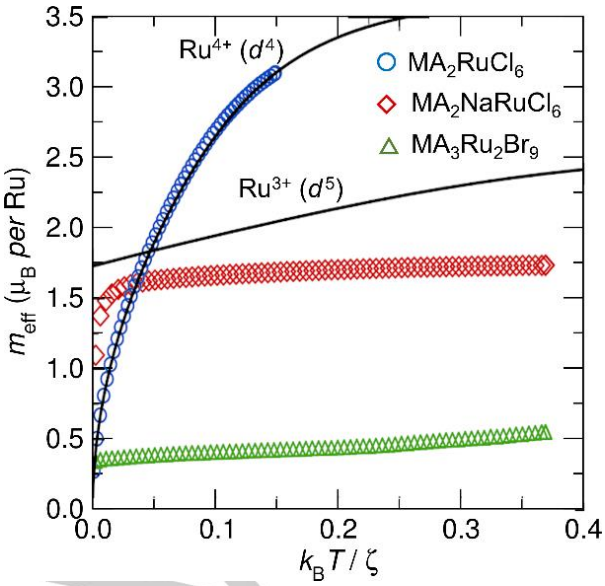

Figure 5. Experimental Kotani plots for MA_2RuCl_6 (**1**), $MA_2NaRuCl_6$ (**3**) and $MA_3Ru_2Br_9$ (**9**). For comparison, the theoretical Kotani plots for Ru^{+4} (d^4) and Ru^{3+} (d^5) single ions are given as black lines.

The six $MA_2M^IRu^{III}X_6$ compounds share the same general formula as the hybrid 3D double perovskites, $A_2M^IM^{III}X_6$, such as MA_2KBiCl_6,[13] MA_2KGdCl_6,[48] MA_2KYCl_6,[48] $MA_2AgBiBr_6$,[12] $MA_2TlBiBr_6$,[11] and MA_2AgSbI_6.[14] However, their structures are entirely different. Compounds **3**-**8** crystallize in the trigonal space group, $P\bar{3}m$, and contain infinite face-sharing chains of octahedral RuX_6 and trigonal-antiprismatic (trigonally elongated pseudo-octahedra) MX_6 polyhedra, interspersed with MA cations (Figure 6, supporting information, Figures S3a and b). Successive RuX_6 octahedra are in a staggered conformation along the *c*-axis. A similar chain structure, $MA_2AgInBr_6$, was recently reported and absorbs in the ultraviolet region.[49] $MA_2AgInBr_6$ comprises face-shared $AgBr_6$ and $InBr_6$ polyhedra. The chains of RuX_6 and MX_6 polyhedra in **3**-**8** are also reminiscent of Sr_4PtO_6, which contains chains of face-sharing octahedral PtO_6 and trigonal prismatic SrO_6.[50] Other examples of 1D perovskite-related transition metal oxides include Ca_3NaRuO_6,[51] Ca_3NiMnO_6,[52] and Sr_3ZnCoO_6.[53] As in **1** and **2**, the RuX_6 octahedra in **3**-**8** are virtually undistorted, with all six Ru-*X* bonds of equal lengths and the *X*-Ru-*X* bond angles very close to 90° and 180° (supporting information, Tables S2, S4 and S5). We again ascribe this finding to the very high ligand field stabilization energy associated with the low spin d^5 Ru^{3+} configuration. The Ru-Cl bond distances in **3**, **4**, and **5** are comparable to those of β-$RuCl_3$ (2.351 Å), which has a $TiCl_3$-type chain structure with face-sharing $RuCl_6$ octahedra.[54] The *a* and *b* axes of the unit cells of chlorides (**3**-**5**) are very similar because of the regularity of the $RuCl_6$ octahedra, so most of the cell volume changes due to the different sizes of the M^+ ions are reflected in the lengths of the *c*-axes (the same is true of the bromides). This leads to the trigonal elongation of the MX_6 octahedra in **3**-**8** along the *c*-axes. Supporting information Figures S3c and d show the dependence of the unit cell volumes and intrachain Ru···Ru distances (*c*-parameters) on the ionic radii of monovalent metals. All the *M*-*X* bonds of each compound are of equal length, but to compensate for the trigonal elongation along the *c*-axis, the *X*-*M*-*X* bond angles deviate significantly from 90º and 180º (supporting information, Tables S2, S4 and S5). The methylammonium cations form N−H···*X* hydrogen bond interactions with the inorganic chains. The shortest donor···acceptor N···Cl distances in **3**, **4** and **5** are ~3.34 Å, while the shortest N···Br distances in **6**-**8** are ~3.50 Å (supporting information, Table S2).

In terms of the optical properties of **3** to **8**, the chlorides, **3**-**5**, show LMCT bands that are typical of isolated $[RuCl_6]^{3-}$ (d^5) complex ion in octahedral coordination.[55,56] Specifically, each of these compounds exhibits four absorption bands in the 5.50-2.25 eV (225-550 nm) range (Figure 7) and they are red in colour. Note that the spectrum of **4** is slightly red-shifted compared to those of **3** and **5**, perhaps due to the role that Ag plays in LMCT for this compound. The bromides **6** and **7** appear black and their spectra are broad (supporting information, Figure S4).

We measured the magnetic susceptibility of $MA_2NaRuCl_6$ (**3**) as a typical representative of this unusual class of chain compounds. **3** has a largely temperature-independent magnetic moment, similar to the Kotani prediction for isolated low-spin d^5 Ru^{3+} ions using a spin-orbit coupling constant ξ of 610 cm^{-1} (Figure 5).[47] Unlike the d^4 Ru^{4+} in **1**, the moment of Ru^{3+} does not become zero at very low temperatures because the ground state is J = 1/2 rather than J = 0. However, the moment is low in comparison with the ideal Kotani behavior that has been reported for isolated RuX_6^{3-} ions.[38] We believe that this arises due to increased exchange interactions resulting from the higher connectivity between $RuCl_6$ within the face-sharing polyhedral chains. Further theoretical development of this intermediate coupling regime is a highly desirable future direction.[57]

Several hybrid $A_3M_2X_9$ compounds (*A* = monovalent organic cation; *M* = trivalent metal ions and *X* = halides) of the main group elements have been studied previously, including $MA_3Sb_2X_9$ (X = Br or I),[58,59] $[C(NH_2)_3]_3M_2I_9$ (*M* = Sb or Bi),[60] $MA_3Bi_2X_9$ (*X* = Br or I).[61] Some of these hybrids adopt $A_3M_2X_9$-type layered structures[62,63] of the type shown in Figure 1, while others contain dimeric $M_2X_9^{3-}$ anions comprising two face-sharing MX_6 octahedra.

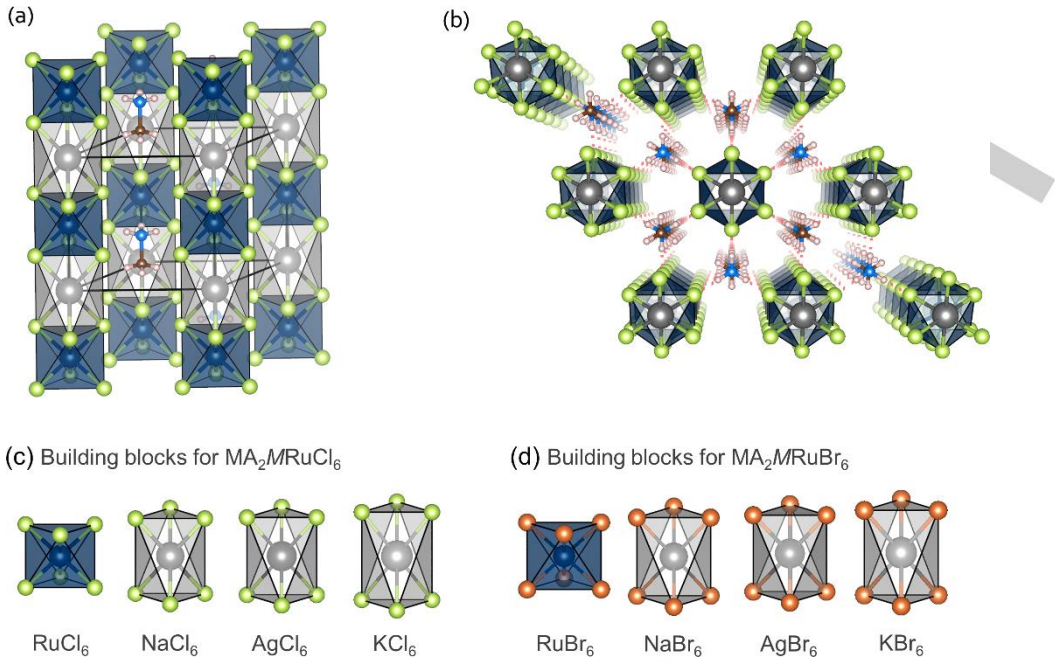

Figure 6. Single-crystal X-ray structure of $MA_2NaRuCl_6$ (**3**). (a) The unit cell showing columns of face-shared $RuCl_6$ and $NaCl_6$ polyhedra connected along the *c*-axis. (b) A perspective view of the X-ray structure showing columns of face-shared $RuCl_6$ and $NaCl_6$ polyhedra, interspersed with methylammonium cations to stabilize the structure by hydrogen bonds with chlorides. The hydrogen bonds are shown by red dotted lines. (c) $RuCl_6$ and MCl_6 (M = Na, Ag or K) polyhedra as the building blocks for the 1D-chains in compounds **3**-**5**. (d) $RuBr_6$ and MBr_6 (M = Na, Ag or K) polyhedra as the building blocks for the 1D-chains in compounds **6**-**8**.

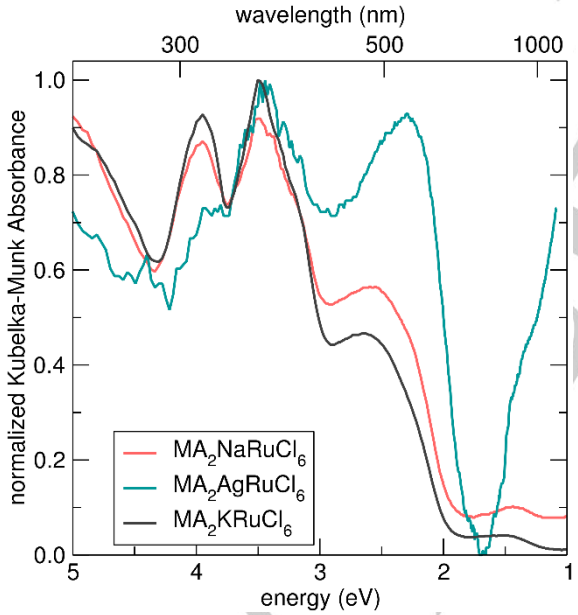

Figure 7. Absorption spectra of $MA_2NaRuCl_6$ (**3**), $MA_2AgRuCl_6$ (**4**) and MA_2KRuCl_6 (**5**).

Compound **9** contains one $[Ru_2Br_9]^{3-}$ dimer oriented along the crystallographic *c*-direction and two crystallographically independent methylammonium cations (Figures 8). One type of methylammonium cation lies in the lateral spaces between the

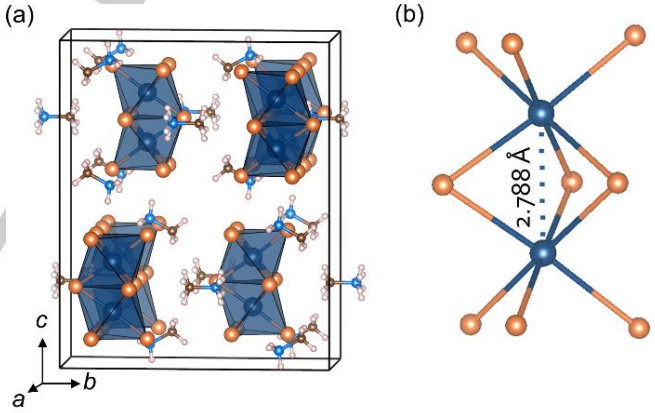

Figure 8. Crystal structure of $MA_3Ru_2Br_9$ (**9**). (a) The unit cell showing $[Ru_2Br_9]^{3-}$ dimers and methylammonium cations. (b) The ball and stick model of $[Ru_2Br_9]^{3-}$ dimer.

dimers, while the other type is present at both ends of the dimers. As in the other compounds described in previous sections, the methylammonium cations form hydrogen bonds with the halide ligands.

Unlike the very regular RuX_6 octahedra in **1** through **8**, the $RuBr_6$ octahedra in **9** are slightly distorted with Br_b-Ru-Br_b bond angles > 90 ° and Br_t-Ru-Br_t bond angles < 90 ° (*b* and *t* indicate bridging and terminal ligands, respectively) (supporting information, Table S6). They also show three slightly different Ru-Br bond distances; Ru-Br_b (2.503 Å×2, 2.483 Å×1) and Ru-Br_t (2.493 Å×2, 2.483 Å×1). The most striking structural feature, however, is the very short Ru···Ru distance (2.789 Å) in the

$[Ru_2Br_9]^{3-}$ dimer (Figure 8b). This bond length is even shorter than the Ru···Ru distance in the previously reported hybrid ruthenium halide phase, [l-ethyl-3-methylimidazolium]$_3Ru_2Br_9$, (2.880 Å).[39] Both of these compounds have M···M distances that are strikingly shorter than those in the $A_3Sb_2X_9$ and $A_3Bi_2X_9$ compounds mentioned earlier, which are typically around 3.3 Å, providing compelling evidence that the ruthenium compounds are exhibiting Ru-Ru bonding. There are several inorganic compounds containing the $Ru_2X_9^{3-}$ dimers that are also believed to exhibit metal-metal bonding. Because of the metal-metal interaction, Ru ions are not at the centers of their octahedra but are slightly displaced towards the center of the dimer. In light of the very high ligand field stabilization energy that would prefer to make the RuX_6 units regular, we must conclude that the Ru-Ru bonding interaction is a significant stabilizing factor. This may be why the dimeric structure appears to be preferred in the hybrid ruthenium compounds, rather than the layered $A_3M_2X_9$ structure.

The optical properties of $MA_3Ru_2Br_9$ (**9**) reveal two intense double bands centered around 4.0 and 2.3 eV (supporting information, Figure S5). These bands arise from LMCT and $\sigma \rightarrow \sigma*$ transitions and are commonly found in Ru^{3+} dimers with significant metal-metal interactions.[56]

The magnetic moment of Ru^{3+} in $MA_3Ru_2Br_9$ deviates substantially from the ideal d^5 Ru^{3+} single-ion behavior (Figure 5), with a dramatically lowered, temperature-independent moment compared to the predicted Kotani behavior for low- spin d^5. This observation cannot be accounted for by changing the spin-orbit coupling constant or adjusting the background from the sample holder within reasonable limits, so we ascribe this lowering of the effective magnetic moment due to metal-metal bonding within the Ru_2Br_9 dimers, as discussed above.

Conclusion

Our study of the methylammonium ruthenium halides has revealed a rich family of new compounds which exhibit three different perovskite-related structures based on Ru^{4+} and Ru^{3+}. The oxidation state of the Ru can be controlled by using H_3PO_2, where appropriate. Two $MA_2Ru^{IV}X_6$ compounds with X = Cl and Br adopt a vacancy-ordered double perovskite structure that is distorted from its idealized cubic symmetry by hydrogen bonding between the MA cations and the halide anions. The magnetic properties of MA_2RuCl_6 are in excellent agreement with the predictions of the Kotani model for low spin d^4 systems exhibiting medium to strong spin-orbit coupling. Six compounds of composition $MA_2MRu^{III}X_6$ (M = Na, K or Ag; X = Cl or Br) adopt a structure containing infinite chains of face-sharing RuX_6 and distorted MX_6 octahedra, rather than the double perovskite structure that is found in systems such as $MA_2M'Bi^{III}X_6$. The magnetic properties of $MA_2NaRu^{III}Cl_6$ deviate from the ideal Kotani model for low spin d^5 systems, probably due to the connectivity between the $RuCl_6$ octahedra within the face-sharing chains. Finally, $MA_3Ru_2Br_9$ adopts a structure containing dimers of face-sharing $RuBr_6$ octahedra, rather than the layered $A_3M_2X_9$ structure that is often found in systems of this general composition. Ru-Ru bonding within the Ru_2Br_9 dimers (Ru–Ru = 2.789 Å) stabilizes the dimeric structure and leads to strong deviations from the Kotani theory. In future work we plan to explore the structures and properties of Ru halide compounds based upon other amine cations.

Acknowledgments

This work is supported by the U. S. Department of Energy, Office of Science, Basic Energy Sciences, under the SC0012541 Grant. The authors acknowledge Materials Research Science and Engineering Center (MRSEC) (Grant No. NSF DMR 1720256) for providing access to its shared facilities created at UC Santa Barbara. PV thanks the Department of Science & Technology (DST), Govt. of India for an Overseas Post-doctoral Visiting Fellowship (Award No. JNC/AO/A.0610-1(3)/2018-03), managed by the Jawaharlal Nehru Centre for Advanced Scientific Research (JNCASR), Bangalore, India. The magnetism aspects of this research was supported by the National Science Foundation (NSF) through the DMREF program DMR 1729489 (JLZ and SDW). JLZ also acknowledges the support of the NSF Graduate Research Fellowship Program under Grant No. 1650114. AKC is grateful to the MOE of Singapore for Tier 1 funding at NUS under grant R284-000-193-114.

Conflict of Interest

There are no conflicts to declare.

Keywords: Lead-free perovskites • double perovskites • ruthenium halides • magnetic properties • Kotani model

[1] A. Kojima, K. Teshima, Y. Shirai, T. Miyasaka, *J. Am. Chem. Soc.* **2009**, *131*, 6050–6051.

[2] M. A. Green, A. Ho-Baillie, H. J. Snaith, *Nat. Photonics* **2014**, *8*, 506–514.

[3] J. Burschka, N. Pellet, S.-J. Moon, R. Humphry-Baker, P. Gao, M. K. Nazeeruddin, M. Grätzel, *Nature* **2013**, *499*, 316–319.

[4] J.-H. Im, I.-H. Jang, N. Pellet, M. Grätzel, N.-G. Park, *Nat. Nanotechnol.* **2014**, *9*, 927–932.

[5] A. G. Kontos, A. Kaltzoglou, M. K. Arfanis, K. M. McCall, C. C. Stoumpos, B. W. Wessels, P. Falaras, M. G. Kanatzidis, *J. Phys. Chem. C* **2018**, *122*, 26353–26361.

[6] N. K. Noel, S. D. Stranks, A. Abate, C. Wehrenfennig, S. Guarnera, A.-A. Haghighirad, A. Sadhanala, G. E. Eperon, S. K. Pathak, M. B. Johnston, et al., *Energy Environ. Sci.* **2014**, *7*, 3061–3068.

[7] Z. Xiao, K.-Z. Du, W. Meng, J. Wang, D. B. Mitzi, Y. Yan, *J. Am. Chem. Soc.* **2017**, *139*, 6054–6057.

[8] C. C. Stoumpos, C. D. Malliakas, M. G. Kanatzidis, *Inorg. Chem.* **2013**, *52*, 9019–9038.

[9] G. Laurita, D. H. Fabini, C. C. Stoumpos, M. G. Kanatzidis, R. Seshadri, *Chem. Sci.* **2017**, *8*, 5628–5635.

[10] A. Wang, Y. Guo, Z. Zhou, X. Niu, Y. Wang, F. Muhammad, H. Li, T. Zhang, J. Wang, S. Nie, et al., *Chem. Sci.* **2019**, *10*, 4573–4579.

[11] Z. Deng, F. Wei, S. Sun, G. Kieslich, A. K. Cheetham, P. D. Bristowe, *J. Mater. Chem. A* **2016**, *4*, 12025–12029.

[12] F. Wei, Z. Deng, S. Sun, F. Zhang, D. M. Evans, G. Kieslich, S. Tominaka, M. A. Carpenter, J. Zhang, P. D. Bristowe, et al., *Chem. Mater.* **2017**, *29*, 1089–1094.

[13] F. Wei, Z. Deng, S. Sun, F. Xie, G. Kieslich, D. M. Evans, M. A. Carpenter, P. D. Bristowe, A. K. Cheetham, *Mater. Horiz.* **2016**, *3*, 328–332.

[14] Y.-J. Li, T. Wu, L. Sun, R.-X. Yang, L. Jiang, P.-F. Cheng, Q.-Q. Hao, T.-J. Wang, R.-F. Lu, W.-Q. Deng, *RSC Adv.* **2017**, *7*, 35175–35180.

[15] X.-N. Hua, J.-X. Gao, X.-G. Chen, P.-F. Li, G.-Q. Mei, W.-Q. Liao, *Dalt. Trans.* **2019**, *48*, 6621–6626.

[16] P.-F. Li, W.-Q. Liao, Y.-Y. Tang, H.-Y. Ye, Y. Zhang, R.-G. Xiong, *J. Am. Chem. Soc.* **2017**, *139*, 8752–8757.

[17] Y.-M. You, W.-Q. Liao, D. Zhao, H.-Y. Ye, Y. Zhang, Q. Zhou, X. Niu, J. Wang, P.-F. Li, D.-W. Fu, et al., *Science (80-.).* **2017**, *357*, 306–309.

[18] W.-Q. Liao, Y.-Y. Tang, P.-F. Li, Y.-M. You, R.-G. Xiong, *J. Am. Chem. Soc.* **2017**, *139*, 18071–18077.

[19] H.-Y. Ye, Y. Zhang, D.-W. Fu, R.-G. Xiong, *Angew. Chemie Int. Ed.* **2014**, *53*, 11242–11247.

[20] A. M. Elseman, A. E. Shalan, S. Sajid, M. M. Rashad, A. M. Hassan, M. Li, *ACS Appl. Mater. Interfaces* **2018**, *10*, 11699–11707.

[21] D. Cortecchia, H. A. Dewi, J. Yin, A. Bruno, S. Chen, T. Baikie, P. P. Boix, M. Grätzel, S. Mhaisalkar, C. Soci, et al., *Inorg. Chem.* **2016**, *55*, 1044–1052.

[22] L. Mao, S. M. L. Teicher, C. C. Stoumpos, R. M. Kennard, R. A. DeCrescent, G. Wu, J. A. Schuller, M. L. Chabinyc, A. K. Cheetham, R. Seshadri, *J. Am. Chem. Soc.* **2019**, *141*, 19099–19109.

[23] I. A. Oxton, O. Knop, J. I. Duncan, *J. Mol. Struct.* **1977**, *38*, 25–32.

[24] H. A. Evans, D. H. Fabini, J. L. Andrews, M. Koerner, M. B. Preefer, G. Wu, F. Wudl, A. K. Cheetham, R. Seshadri, *Inorg. Chem.* **2018**, *57*, 10375–10382.

[25] F. Funabiki, Y. Toda, H. Hosono, *J. Phys. Chem. C* **2018**, *122*, 10749–10754.

[26] K. Ishida, H. Mukuda, Y. Kitaoka, K. Asayama, Z. Q. Mao, Y. Mori, Y. Maeno, *Nature* **1998**, *396*, 658–660.

[27] O. Gingras, R. Nourafkan, A.-M. S. Tremblay, M. Côté, *Phys. Rev. Lett.* **2019**, *123*, 217005.

[28] J. Xia, W. Siemons, G. Koster, M. R. Beasley, A. Kapitulnik, *Phys. Rev. B* **2009**, *79*, 140407.

[29] S. Woo, S. A. Lee, H. Mun, Y. G. Choi, C. J. Zhung, S. Shin, M. Lacotte, A. David, W. Prellier, T. Park, et al., *Nanoscale* **2018**, *10*, 4377–4384.

[30] I. Qasim, P. E. R. Blanchard, K. S. Knight, J. Ting, B. J. Kennedy, *Dalt. Trans.* **2019**, *48*, 4730–4741.

[31] W. Witczak-Krempa, G. Chen, Y. B. Kim, L. Balents, *Annu. Rev. Condens. Matter Phys.* **2014**, *5*, 57–82.

[32] A. Banerjee, C. A. Bridges, J.-Q. Yan, A. A. Aczel, L. Li, M. B. Stone, G. E. Granroth, M. D. Lumsden, Y. Yiu, J. Knolle, et al., *Nat. Mater.* **2016**, *15*, 733–740.

[33] A. Kitaev, *Ann. Phys. (N. Y).* **2006**, *321*, 2–111.

[34] S. Mashhadi, D. Weber, L. M. Schoop, A. Schulz, B. V Lotsch, M. Burghard, K. Kern, *Nano Lett.* **2018**, *18*, 3203–3208.

[35] D. Weber, L. M. Schoop, V. Duppel, J. M. Lippmann, J. Nuss, B. V Lotsch, *Nano Lett.* **2016**, *16*, 3578–3584.

[36] R. B. Johannesen, G. A. Candela, *Inorg. Chem.* **1963**, *2*, 67–72.

[37] A. Earnshaw, B. N. Figgis, J. Lewis, R. D. Peacock, *J. Chem. Soc.* **1961**, 3132–3138.

[38] H. Lu, J. R. Chamorro, C. Wan, T. M. McQueen, *Inorg. Chem.* **2018**, *57*, 14443–14449.

[39] D. Appleby, P. B. Hitchcock, K. R. Seddon, J. E. Turp, J. A. Zora, C. L. Hussey, J. R. Sanders, T. A. Ryan, *J. Chem. Soc. Dalt. Trans.* **1990**, 1879–1887.

[40] M. Kotani, *J. Phys. Soc. Japan* **1949**, *4*, 293–297.

[41] A. Earnshaw, B. N. Figgis, J. Lewis, R. S. Nyholm, *Nature* **1957**, *179*, 1121–1124.

[42] A. E. Maughan, A. M. Ganose, D. O. Scanlon, J. R. Neilson, *Chem. Mater.* **2019**, *31*, 1184–1195.

[43] I. Pabst, H. Fuess, J. W. Bats, *Acta Crystallogr. Sect. C Cryst. Struct. Commun.* **1987**, *43*, 413–416.

[44] R. Willett, H. Place, M. Middleton, *J. Am. Chem. Soc.* **1988**, *110*, 8639–8650.

[45] T. Steiner, *Acta Crystallogr. Sect. B* **1998**, *54*, 456–463.

[46] A. Jabłońska-Wawrzycka, P. Rogala, S. Michałkiewicz, M. Hodorowicz, B. Barszcz, *Dalt. Trans.* **2013**, *42*, 6092–6101.

[47] B. N. Figgis, J. Lewis, R. S. Nyholm, R. D. Peacock, *Discuss. Faraday Soc.* **1958**, *26*, 103–109.

[48] Z. Deng, F. Wei, F. Brivio, Y. Wu, S. Sun, P. D. Bristowe, A. K. Cheetham, *J. Phys. Chem. Lett.* **2017**, *8*, 5015–5020.

[49] T. T. Tran, M. A. Quintero, K. E. Arpino, Z. A. Kelly, J. R. Panella, X. Wang, T. M. McQueen, *CrystEngComm* **2018**, *20*, 5929–5934.

[50] A. P. Wilkinson, A. K. Cheetham, W. Kunnman, A. Kvick, *Eur. J. Solid State Inorg. Chem.* **1991**, *28*, 453−459.

[51] J. B. Claridge, R. C. Layland, R. D. Adams, H.-C. zur Loye, *Zeitschrift für Anorg. und Allg. Chemie* **1997**, *623*, 1131–1134.

[52] S. Kawasaki, M. Takano, T. Inami, *J. Solid State Chem.* **1999**, *145*, 302–308.

[53] X. Wang, Y. Guo, Y. Sun, Y. Tsujimoto, Y. Matsushita, K. Yamaura, *J. Solid State Chem.* **2013**, *204*, 40–46.

[54] J. M. Fletcher, W. E. Gardner, A. C. Fox, G. Topping, *J. Chem. Soc. A* **1967**, 1038–1045.

[55] B. E. Bursten, F. A. Cotton, A. Fang, *Inorg. Chem.* **1983**, *22*, 2127–2133.

[56] G. A. Heath, J. E. McGrady, *J. Chem. Soc. Dalt. Trans.* **1994**, 3759–3767.

[57] G. Chen, L. Balents, A. P. Schnyder, *Phys. Rev. Lett.* **2009**, *102*, 96406.

[58] T. Kawai, E. Takao, S. Shimanuki, M. Iwata, A. Miyashita, Y. Ishibashi, *J. Phys. Soc. Japan* **1999**, *68*, 2848–2856.

[59] J. Zaleski, R. Jakubas, L. Sobczyk, J. Mróz, *Ferroelectrics* **1990**, *103*, 83–90.

[60] P. Szklarz, A. Pietraszko, R. Jakubas, G. Bator, P. Zieliński, M. Gałazka, *J. Phys. Condens. Matter* **2008**, *20*, 255221.

[61] M. E. Kamminga, A. Stroppa, S. Picozzi, M. Chislov, I. A. Zvereva, J. Baas, A. Meetsma, G. R. Blake, T. T. M. Palstra, *Inorg. Chem.* **2017**, *56*, 33–41.

[62] P. Szklarz, J. Zaleski, R. Jakubas, G. Bator, W. Medycki, K. Falińska, *J. Phys. Condens. Matter* **2005**, *17*, 2509–2528.

[63] J. Zaleski, C. Pawlaczyk, R. Jakubas, H.-G. Unruh, *J. Phys. Condens. Matter* **2000**, *12*, 7509–7521.

Entry for the Table of Contents

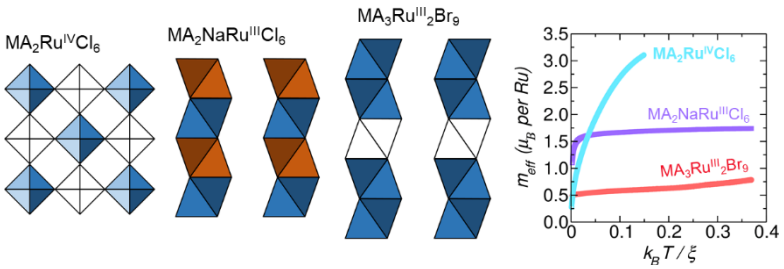

Three families of structurally diverse methylammonium ruthenium halide perovskites and related compounds have been synthesized for the first time: MA_2RuX_6 (X = Cl or Br), MA_2MRuX_6 (M = Na, K or Ag; X = Cl or Br) and $MA_3Ru_2X_9$ (X = Br). The effective magnetic moments of these compounds decrease in the order $MA_2RuX_6 > MA_2MRuX_6 > MA_3Ru_2X_9$.

Institute and/or researcher Twitter usernames: ((optional))

Table of contents

Experimental section

Materials and Methods. Methylammonium chloride (Sigma Aldrich), methylammonium bromide (Sigma Aldrich), NaCl (Merck), KCl (Merck), AgCl (Merck), NaBr (Merck), anhydrous $RuCl_3$ (Alfa Easar), 37 wt. % HCl in H_2O (Merck), 48 wt. % HBr in H_2O (Sigma Aldrich), 50 wt. % H_3PO_2 in H_2O (Sigma Aldrich) were purchased from commercial sources and used as received. All the compounds were synthesized hydrothermally in 23 mL Teflon-lined autoclave. The crystals were separated by filtration, washed several times with ethanol and dried under vacuum.

Synthesis of MA_2RuCl_6 (1). A mixture of methylammonium chloride (135.0 mg, 2.0 mmol), $RuCl_3$ (207.43 mg, 1.0 mmol) and HCl (2.0 mL, 37 wt% in H_2O) was heated at 160 ℃ for 48 h in a 23 mL Teflon-lined autoclave in an oven. The autoclave was allowed to cool to room temperature which yielded dark red crystals of **1**. Yield; 300 mg (79.3 %, calculated based on $RuCl_3$ used).

Synthesis of MA_2RuBr_6 (2). A mixture of methylammonium bromide (223.95 mg, 2.0 mmol), $RuCl_3$ (207.43 mg, 1.0 mmol) and HBr (2.0 mL, 48 wt % in H_2O, Sigma Aldrich) was heated at 160 ℃ for 48 h in a 23 mL Teflon-lined autoclave in an oven. The autoclave was allowed to cool to room temperature which yielded black crystals of **2**. Yield; 550 mg (85.3 %, calculated based on $RuCl_3$ used).

Synthesis of $MA_2NaRuCl_6$ (3). A mixture of methylammonium chloride (67.50 mg, 1.0 mmol), NaCl (29.22 mg, 0.5 mmol), $RuCl_3$ (103.71 mg, 0.5 mmol), HCl (1.5 mL, 37 wt % in H_2O) and H_3PO_2 (66.0 mg of 50 wt% in H_2O, 0.5 mmol) was heated at 160 ℃ for 48 h in a 23 mL Teflon-lined autoclave in an oven. After heating for 48 h, the autoclave was allowed to cool to room temperature which yielded red plate-like hexagonal crystals of **3**. Yield; 75 mg (37.4 %, calculated based on $RuCl_3$ used).

Synthesis of $MA_2AgRuCl_6$ (4). A mixture of methylammonium chloride (67.50 mg, 1.0 mmol), AgCl (71.66 mg, 0.5 mmol), $RuCl_3$ (103.71 mg, 0.5 mmol), HCl (1.50 mL, 37 wt % in H_2O) and H_3PO_2 (66.0 mg of 50 wt% in H_2O, 0.5 mmol) was heated at 160 ℃ for 48 h in a 23 mL Teflon-lined autoclave in an oven. The autoclave was allowed to cool to room temperature which yielded plate-like hexagonal dark red crystals of **4**. Yield; 92 mg (38 %, calculated based on $RuCl_3$ used).

Synthesis of MA_2KRuCl_6 (5). A mixture of methylammonium chloride (67.50 mg, 1.0 mmol), KCl (37.27 mg, 0.5 mmol), $RuCl_3$ (103.71 mg, 0.5 mmol), HCl (1.50 mL, 37 wt % in H_2O)

and H_3PO_2 (66.0 mg of 50 wt% in H_2O, 0.5 mmol) was heated at 160 °C for 48 h in a 23 mL Teflon-lined autoclave in an oven. The autoclave was allowed to cool to room temperature which yielded red thin flake-like red crystals of **5**. Yield; 80 mg (38.5 %, calculated based on $RuCl_3$ used).

Synthesis of $MA_2NaRuBr_6$ (6). A mixture of methylammonium bromide (111.97 mg, 1.0 mmol), NaBr (51.45 mg, 0.5 mmol), $RuCl_3$ (103.71 mg, 0.5 mmol), HBr (1.50 mL, 37 wt % in H_2O) and H_3PO_2 (66.0 mg of 50 wt% in H_2O, 0.5 mmol) was heated at 160 °C for 48 h in a 23 mL Teflon-lined autoclave in an oven. The autoclave was allowed to cool to room temperature which yielded black crystals of **6**. Yield; 100 mg (30 %, calculated based on $RuCl_3$ used).

Synthesis of $MA_2AgRuBr_6$ (7). A mixture of methylammonium bromide (111.97 mg, 1.0 mmol), AgCl (71.66 mg, 0.5 mmol), $RuCl_3$ (103.71 mg, 0.5 mmol), HBr (1.50 mL, 37 wt % in H_2O) and H_3PO_2 (66.0 mg of 50 wt% in H_2O, 0.5 mmol) was heated at 160 °C for 48 h in a 23 mL Teflon-lined autoclave in an oven. The autoclave was allowed to cool to room temperature. Dark red crystals of **7** were obtained at the bottom of the vessel. Yield; 150 mg (39.9%, calculated based on $RuCl_3$ used).

Syntheses of MA_2KRuBr_6 (8) and $MA_3Ru_2Br_9$ (9). A mixture of methylammonium bromide (111.97 mg, 1.0 mmol), KCl (37.27 mg, 0.5 mmol), $RuCl_3$ (103.71 mg, 0.5 mmol), HBr (1.50 mL, 37 wt % in H_2O) and H_3PO_2 (66.0 mg of 50 wt% in H_2O, 0.5 mmol) was heated at 160 °C for 48 h in a 23 mL Teflon-lined autoclave in an oven. After heating for 48 h, the autoclave was allowed to cool to room temperature which yielded dark red polycrystalline powder of **9** which was separated by filtration. The dark red filtrate was kept at room temperature. A mixture of hexagonal dark red crystals of **8** and needle-like black crystals of **9** were obtained after 2 days. The crystals were filtered out and the filtrate was again kept for crystallization. One type of needle-like crystals of **9** were obtained in 2 days.

Single crystal X-ray diffraction. Room temperature single-crystal X-ray diffraction data were collected on a Bruker Kappa Apex II diffractometer equipped with an APEX II CCD detector and a TRIUMPH monochromator with Mo-Kα X-ray source (wavelength = 0.71073 Å) in ω-scan mode. The data collection and integration were carried out with APEX3 software. The structures were solved by direct methods and refined by full-matrix least-squares on F^2 by using the *SHELXL-2014* program package.[1] The non-hydrogen atoms were located from the electron density found in the difference maps and refined anisotropically. The hydrogen atoms of methylammonium cations were placed in their geometrically idealized positions and refined with isotopic parameters as

riding atoms. The structures were drawn from CIFs by using the VESTA (version 3) software.

Powder X-ray diffraction. Powder diffraction data were obtained on a Panalytical Empyrean powder diffractometer equipped with a Cu-Kα X-ray source (wavelength = 1.54056 Å). The experimental PXRD patterns were compared with the patterns simulated from the CIFs from single-crystal X-ray diffraction data (see Supplementary Information) in order to verify the phase purity of the bulk samples (Figures S6-S14).

Thermogravimetric analysis (TGA). TGA of all compounds was carried out under continuous flow of nitrogen gas (flow rate; 25 mL/minute) on a Discovery TGA instrument (TA Instruments). The samples (5-6 mg) were heated in aluminum crucibles at a temperature ramp rate of 10 °C min^{-1} (Figures S15-S23).

Optical properties. Diffuse reflectance spectra were measured in the wavelength range of 220–2600 nm on a Shimadzu UV-3600 UV–vis–NIR spectrometer. $BaSO_4$ (Sigma Aldrich) was used as the reference (100% reflectance) as well as for dilution of the samples. The samples were prepared by mixing each compound with $BaSO_4$ in a 1:3 ratio. The diffuse reflectance data were converted to absorbance by using the Kubelka–Munk (K-M) expression,

$$\frac{k}{s} = \frac{(1-R)^2}{(2R)}$$

where k is the absorption coefficient, s is the scattering coefficient and R is the reflectance. It is generally assumed that s is a constant and it is independent of wavelength. Therefore, the k/s term is assumed to be equivalent to the absorption coefficient.

Magnetic properties. Magnetic susceptibility measurements were collected for compounds **1**, **3** and **9** on a Quantum Design MPMS3 SQUID magnetometer. In each case, approximately 15 mg of powder sample was mounted on a brass holder in plastic caps. Zero field-cooled (ZFC) and field-cooled (FC) susceptibility versus temperature measurements were performed in the 2 to 300K range. We used the Curie law,

$$m_{eff} = \sqrt{\frac{3k_B}{N_A\mu_B^2}\chi T}$$

to transform the molar magnetic susceptibilities (χ) into the effective magnetic moments (m_{eff}), where k_B is the Boltzmann constant, χ is the molar susceptibilities, T is the temperature, N_A is Avogadro's number and μ_B is Bohr magneton

Table S1. Details of X-ray data collection and the structure refinement of MA_2RuX_6 (**1** and **2**), MA_2MRuX_6 (**3**-**8**) and $MA_3Ru_2Br_9$ (**9**).

	MA_2RuCl_6 (1)	**MA_2RuBr_6 (2)**	**$MA_2NaRuCl_6$ (3)**
CCDC Number	1982755	1982756	1982757
Empirical formula	$H_{12}C_2N_2RuCl_6$	$H_{12}C_2N_2RuBr_6$	$H_{12}C_2N_2NaRuCl_6$
Formula weight	377.91	644.67	400.90
Temperature (K)	299(2)	299(2)	299(2)
Wavelength (Å)	0.71073	0.71073	0.71073
Crystal system	Trigonal	Trigonal	Trigonal
Space group	$R\bar{3}m1$	$R\bar{3}m1$	$P\bar{3}m1$
Unit cell dimensions			
a (Å)	6.9935(3)	7.3485(10)	7.2493(9)
b (Å)	6.9935(3)	7.3485(10)	7.2493(9)
c (Å)	21.9740(12)	22.376(4)	6.7926(8)
α (°)	90	90	90
β (°)	90	90	90
γ (°)	120	120	120
V (Å^3)	930.74(9)	1046.4(3)	309.14(8)
Z	3	3	1
Calc. density (mg/m^3)	2.023	3.069	2.153
Absorption coeff. (mm^{-1})	2.507	18.265	2.553
Crystal size (mm^3)	0.200 x 0.150 x 0.100	0.200 x 0.050 x 0.050	0.15 x 0.15 x 0.05
θ range for data collection (°)	2.781 to 26.968	2.731 to 27.943	2.999 to 30.386
Reflections collected	2626	2469	2640
Independent reflections	287 [R(int) = 0.0128]	351 [R(int) = 0.0943]	385 [R(int) = 0.0425]
Completeness to 2θ = 25.242° (%)	100.0	100.0	100.0
Data / restraints / parameters	287 /3 / 21	351 / 4 / 20	385 / 2 / 23
Goodness-of-fit	1.200	1.148	1.190
Final R indices [I>2sigma(I)]	$R1$ = 0.0127, $wR2$ = 0.0338	$R1$ = 0.0437, $wR2$ = 0.1035	$R1$ = 0.0195, $wR2$ = 0.0482
R indices (all data)	$R1$ = 0.0128, $wR2$ = 0.0340	$R1$ = 0.0546, $wR2$ = 0.1089	$R1$ = 0.0214, $wR2$ = 0.0496
Largest diff. peak and hole	0.201 and -0.389 e.Å^{-3}	1.470 and -0.905 e.Å^{-3}	0.384 and -0.641 e.Å^{-3}

	$MA_2AgRuCl_6$ (4)	**MA_2KRuCl_6 (5)**	**$MA_2NaRuBr_6$ (6)**
CCDC Number	1982758	1982759	1982760
Empirical formula	$H_{12}C_2N_2AgRuCl_6$	$H_{12}C_2N_2KRuCl_6$	$H_{12}C_2N_2NaRuBr_6$
Formula weight	485.78	417.01	667.66
Temperature (K)	299(2)	293(2)	300(2)
Wavelength (Å)	0.71073	0.71073	0.71073
Crystal system	Trigonal	Trigonal	Trigonal
Space group	$P\bar{3}m1$	$P\bar{3}m1$	$P\bar{3}m1$
Unit cell dimensions			
a (Å)	7.237(5)	7.181(5)	7.561(5)
b (Å)	7.237(5)	7.181(5)	7.561(5)
c (Å)	6.936(5)	7.366(5)	7.105(5)
α (°)	90	90	90
β (°)	90	90	90
γ (°)	120	120	120
V (Å^3)	314.6(5)	329.0(5)	351.8(5)
Z	1	1	1
Calc. density (mg/m^3)	2.564	2.105	3.152
Absorption coeff. (mm^{-1})	3.986	2.683	18.144
Crystal size (mm^3)	0.200 x 0.100 x 0.020	0.150 x 0.150 x 0.050	0.200 x 0.100 x 0.050
θ range for data collection (°)	3.251 to 30.321	2.765 to 28.260	2.867 to 26.293
Reflections collected	1451	1597	1094
Independent reflections	381 [R(int) = 0.0436]	338 [R(int) = 0.0349]	300 [R(int) = 0.0543]

Completeness to 2θ = 25.242° (%)	96.8	98.4	100.0
Data / restraints / parameters	381 / 4 / 20	338 / 4 / 23	300 / 4 / 24
Goodness-of-fit	1.150	1.156	1.165
Final R indices [I>2sigma(I)]	*R*1 = 0.0368, *wR*2 = 0.0960	*R*1 = 0.0244, *wR*2 = 0.0687	*R*1 = 0.0588, *wR*2 = 0.1664
R indices (all data)	*R*1 = 0.0398, *wR*2 = 0.1013	*R*1 = 0.0282, *wR*2 = 0.0737	*R*1 = 0.0646, *wR*2 = 0.1727
Largest diff. peak and hole	0.378 and -0.407 e.Å^{-3}	2.018 and -1.989 e.Å^{-3}	
	1.018 and -1.202		

	$MA_2AgRuBr_6$ (7)	**MA_2KRuBr_6 (8)**	**$MA_3Ru_2Br_9$ (9)**
CCDC Number	1982761	1982762	1982763
Empirical formula	$H_{12}C_2N_2AgRuBr_6$	$H_{12}C_2N_2KRuBr_6$	$H_{18}C_3Br_9N_3Ru_2$
Formula weight	752.54	683.77	1017.53
Temperature (K)	299(2)	299(2)	299(2)
Wavelength (Å)	0.71073	0.71073	0.71073
Crystal system	Trigonal	Trigonal	Orthorhombic
Space group	$P\bar{3}m1$	$P\bar{3}m1$	*C*mcm
Unit cell dimensions			
a (Å)	7.516(5)	7.4892(17)	7.3797(16)
b (Å)	7.516(5)	7.4892(17)	15.167(4)
c (Å)	7.032(4)	7.3894(18)	18.419(5)
α (°)	90	90	90
β (°)	90	90	90
γ (°)	120	120	90
V (Å^3) 7.516(5)	344.1(5)	358.93(18)	2061.6(9)
Z	1	1	4
Calc. density (mg/m^3)	3.632	3.163	3.278
Absorption coeff. (mm^{-1})	19.901	18.042	18.895
Crystal size (mm^3)	0.20 x 0.20 x 0.05	0.25 x 0.15 x 0.05	0.100 x 0.100 x 0.050
θ range for data collection (°)	3.130 to 25.989	2.756 to 26.449	2.211 to 27.646
Reflections collected	726	812	5382
Independent reflections	286 [R(int) = 0.0698]	310 [R(int) = 0.0379]	1320 [R(int) = 0.1452]
Completeness to 2θ = 25.242° (%)	99.6	100.0	99.8
Data / restraints / parameters	286 / 4 / 22	310 / 4 / 23	1320 / 74 / 73
Goodness-of-fit	1.038	1.023	1.077
Final R indices [I>2sigma(I)]	*R*1 = 0.0554, *wR*2 = 0.1322	*R*1 = 0.0371, *wR*2 = 0.0685	*R*1 = 0.0532, *wR*2 = 0.0730
R indices (all data)	*R*1 = 0.0830, *wR*2 = 0.1469	*R*1 = 0.0621, *wR*2 = 0.0753	*R*1 = 0.1475, *wR*2 = 0.0903
Largest diff. peak and hole	1.504 and -1.905 e.Å^{-3}	1.048 and -1.035 e.Å^{-3}	1.254 and -1.131 e.Å^{-3}

Table S2. Selected bond distances for $MA_2Ru\mathit{X}_6$ (**1** and **2**), $MA_2\mathit{M}Ru\mathit{X}_6$ (**3**-**8**) and $MA_3Ru_2Br_9$ (**9**) obtained from the single-crystal X-ray diffraction data.

Compounds	**Distances (Å)**			
	Ru···Ru	**Ru-*X***	***M*-*X***	**N···*X***
MA_2RuCl_6 (**1**)	6.994	2.327(1)×6	-	3.432×1, 3.499×2
MA_2RuBr_6 (**2**)	7.349	2.483(1)×6	-	3.568×1, 3.676×2
$MA_2NaRuCl_6$ (**3**)	6.793 (intra-chains), 7.249 (inter-chains)	2.374(5)×6	2.794(6)×6	3.340×1, 3.640×2
$MA_2AgRuCl_6$ (**4**)	6.936 (intra-chains), 7.237 (inter-chains)	2.394(2)×6	2.825(2)×6	3.414×1, 3.630×2
MA_2KRuCl_6 (**5**)	7.366 (intra-chains), 7.181 (inter-chains)	2.383(2)×6	3.035(2)×6	3.344×1, 3.597×2
$MA_2NaRuBr_6$ (**6**)	7.105 (intra-chains), 7.561 (inter-chains)	2.521(2)×6	2.937(2)×6	3.504×1, 3.792×2
$MA_2AgRuBr_6$ (**7**)	7.032 (intra-chains), 7.516 (inter-chains)	2.509(2)×6	2.893(2)×6	3.495×1, 3.772×2
MA_2KRuBr_6 (**8**)	7.389 (intra-chains), 7.489 (inter-chains)	2.513(1)×6	3.058(1)×6	3.505×1, 3.751×2
$MA_3KRu_2Br_9$ (**9**)	2.789(3)	2.481(3)×2	-	3.453×1, 3.490×2
		2.483(3)×1		
		2.494(2)×2		
		2.499(2)×3		

Table S3. Selected bond angles (°) for **1** and **2**.

MA_2RuCl_6 (1)		**MA_2RuBr_6 (2)**	
∠Cl-Ru-Cl		**∠Br-Ru-Br**	
Cl(1)#1-Ru(1)-Cl(1)#2	90.342(14)	Br(1)#1-Ru(1)-Br(1)#2	90.07(3)

Cl(1)#1-Ru(1)-Cl(1)	89.660(14)	Br(1)#1-Ru(1)-Br(1)	89.93(3)
Cl(1)#2-Ru(1)-Cl(1)	89.660(14)	Br(1)#2-Ru(1)-Br(1)	89.93(3)
Cl(1)#1-Ru(1)-Cl(1)#3	180.0	Br(1)#1-Ru(1)-Br(1)#3	180.0
Cl(1)#2-Ru(1)-Cl(1)#3	89.659(14)	Br(1)#2-Ru(1)-Br(1)#3	89.93(3)
Cl(1)-Ru(1)-Cl(1)#3	90.340(14)	Br(1)-Ru(1)-Br(1)#3	90.07(3)
Cl(1)#1-Ru(1)-Cl(1)#4	90.341(14)	Br(1)#1-Ru(1)-Br(1)#4	90.07(3)
Cl(1)#2-Ru(1)-Cl(1)#4	90.342(14)	Br(1)#2-Ru(1)-Br(1)#4	90.07(3)
Cl(1)-Ru(1)-Cl(1)#4	180.0	Br(1)-Ru(1)-Br(1)#4	180.00
Cl(1)#3-Ru(1)-Cl(1)#4	89.659(14)	Br(1)#3-Ru(1)-Br(1)#4	89.93(3)
Cl(1)#1-Ru(1)-Cl(1)#5	89.659(14)	Br(1)#1-Ru(1)-Br(1)#5	89.93(3)
Cl(1)#2-Ru(1)-Cl(1)#5	180.0	Br(1)#2-Ru(1)-Br(1)#5	180.0
Cl(1)-Ru(1)-Cl(1)#5	90.340(14)	Br(1)-Ru(1)-Br(1)#5	90.07(3)
Cl(1)#3-Ru(1)-Cl(1)#5	90.340(14)	Br(1)#3-Ru(1)-Br(1)#5	90.06(3)
Cl(1)#4-Ru(1)-Cl(1)#5	89.659(14)	Br(1)#4-Ru(1)-Br(1)#5	89.93(3)
Symmetry transformations used to generate equivalent atoms: #1 y+1/3,-x+y+2/3,-z+2/3 #2 x-y+1/3,x-1/3,-z+2/3 #3 -y+1,x-y,z #4 -x+4/3,-y+2/3,-z+2/3 #5 -x+y+1,-x+1,z		Symmetry transformations used to generate equivalent atoms: #1 y+1/3,-x+y+2/3,-z+2/3 #2 x-y+1/3,x-1/3,-z+2/3 #3 -y+1,x-y,z #4 -x+4/3,-y+2/3,-z+2/3 #5 -x+y+1,-x+1,z #6 -y+1,x-y+1,z #7 -x+y,-x+1,z	

Table S4. Selected bond angles (°) for **3**-**5**.

$MA_2NaRuCl_6$ (3)			
∠Cl-Ru-Cl		**∠Cl-Na-Cl**	
Cl(1)#1-Ru(1)-Cl(1)#2	180.0	Cl(1)#2-Na(1)-Cl(1)	73.605(17)
Cl(1)#1-Ru(1)-Cl(1)	90.33(2)	Cl(1)#7-Na(1)-Cl(1)#8	73.606(17)
Cl(1)#2-Ru(1)-Cl(1)	89.67(2)	Cl(1)-Na(1)-Cl(1)#4	73.605(17)
Cl(1)#1-Ru(1)-Cl(1)#3	89.67(2)	Cl(1)#7-Na(1)-Cl(1)#9	73.606(17)
Cl(1)#2-Ru(1)-Cl(1)#3	90.33(2)	Cl(1)#2-Na(1)-Cl(1)#4	73.606(17)
Cl(1)-Ru(1)-Cl(1)#3	180.0	Cl(1)#8-Na(1)-Cl(1)#9	73.605(17)
Cl(1)#1-Ru(1)-Cl(1)#4	90.33(2)	Cl(1)#7-Na(1)-Cl(1)	106.395(17)
Cl(1)#2-Ru(1)-Cl(1)#4	89.67(2)	Cl(1)#2-Na(1)-Cl(1)#8	106.394(17)
Cl(1)-Ru(1)-Cl(1)#4	89.67(2)	Cl(1)-Na(1)-Cl(1)#8	106.395(17)
Cl(1)#3-Ru(1)-Cl(1)#4	90.33(2)	Cl(1)#7-Na(1)-Cl(1)#4	106.394(17)
Cl(1)#1-Ru(1)-Cl(1)#5	89.67(2)	Cl(1)#2-Na(1)-Cl(1)#9	106.394(17)
Cl(1)#2-Ru(1)-Cl(1)#5	90.33(2)	Cl(1)#4-Na(1)-Cl(1)#9	106.395(17)
Cl(1)-Ru(1)-Cl(1)#5	90.33(2)	Symmetry transformations used to generate equivalent atoms: #1 x-y,x,-z+1 #2 -x+y,-x,z #3 -x,-y,-z+1 #4 -y,x-y,z #5 y,-x+y,-z+1 #6 x,y,z-1 #7 x-y,x,-z+2 #8 y,-x+y,-z+2 #9 -x,-y,-z+2 #10 x,y,z+1	
Cl(1)#3-Ru(1)-Cl(1)#5	89.67(2)		
Cl(1)#4-Ru(1)-Cl(1)#5	180.0		
$MA_2AgRuCl_6$ (4)			
∠Cl-Ru-Cl		**∠Cl-Ag-Cl**	
Cl(1)-Ru(1)-Cl(1)#1	180.00	Cl(1)#6-Ag(1)-Cl(1)#7	72.78(5)
Cl(1)-Ru(1)-Cl(1)#2	91.15(6)	Cl(1)#3-Ag(1)-Cl(1)	72.78(5)
Cl(1)#1-Ru(1)-Cl(1)#2	88.85(6)	Cl(1)#6-Ag(1)-Cl(1)#8	72.78(5)
Cl(1)-Ru(1)-Cl(1)#3	88.85(6)	Cl(1)#7-Ag(1)-Cl(1)#8	72.78(5)
Cl(1)#1-Ru(1)-Cl(1)#3	91.15(6)	Cl(1)#3-Ag(1)-Cl(1)#4	72.78(5)
Cl(1)#2-Ru(1)-Cl(1)#3	180.00	Cl(1)-Ag(1)-Cl(1)#4	72.78(5)
Cl(1)-Ru(1)-Cl(1)#4	88.85(6)	Cl(1)#3-Ag(1)-Cl(1)#7	107.22(5)
Cl(1)#1-Ru(1)-Cl(1)#4	91.15(6)	Cl(1)#6-Ag(1)-Cl(1)	107.22(5)
Cl(1)#2-Ru(1)-Cl(1)#4	91.15(6)	Cl(1)#3-Ag(1)-Cl(1)#8	107.22(5)
Cl(1)#3-Ru(1)-Cl(1)#4	88.85(6)	Cl(1)-Ag(1)-Cl(1)#8	107.22(5)
Cl(1)-Ru(1)-Cl(1)#5	91.15(6)	Cl(1)#6-Ag(1)-Cl(1)#4	107.22(5)
Cl(1)#1-Ru(1)-Cl(1)#5	88.85(6)	Cl(1)#7-Ag(1)-Cl(1)#4	107.22(5)
Cl(1)#2-Ru(1)-Cl(1)#5	88.85(6)	Symmetry transformations used to generate equivalent atoms: #1 -x,-y,-z+1 #2 x-y,x,-z+1 #3 -x+y,-x,z #4 -y,x-y,z #5 y,-x+y,-z+1 #6 x-y,x,-z+2 #7 -x,-y,-z+2	
Cl(1)#3-Ru(1)-Cl(1)#5	91.15(6)		
Cl(1)#4-Ru(1)-Cl(1)#5	180.0		

Cl(1)#6-Ag(1)-Cl(1)#3	180.0	#8 y,-x+y,-z+2

MA_2KRuCl_6 (5)

∠Cl-Ru-Cl		**∠Cl-K-Cl**	
Cl(1)#1-Ru(1)-Cl(1)#2	180.00	Cl(1)#4-K(1)-Cl(1)#3	67.83(5)
Cl(1)#1-Ru(1)-Cl(1)#3	90.61(5)	Cl(1)#7-K(1)-Cl(1)#8	67.83(5)
Cl(1)#2-Ru(1)-Cl(1)#3	89.39(5)	Cl(1)#4-K(1)-Cl(1)#1	67.83(5)
Cl(1)#1-Ru(1)-Cl(1)#4	90.61(5)	Cl(1)#3-K(1)-Cl(1)#1	67.83(5)
Cl(1)#2-Ru(1)-Cl(1)#4	89.39(5)	Cl(1)#7-K(1)-Cl(1)#9	67.83(5)
Cl(1)#3-Ru(1)-Cl(1)#4	90.61(5)	Cl(1)#8-K(1)-Cl(1)#9	67.83(5)
Cl(1)#1-Ru(1)-Cl(1)#5	89.39(5)	Cl(1)#7-K(1)-Cl(1)#3	112.17(5)
Cl(1)#2-Ru(1)-Cl(1)#5	90.61(5)	Cl(1)#4-K(1)-Cl(1)#8	112.17(5)
Cl(1)#3-Ru(1)-Cl(1)#5	89.39(5)	Cl(1)#7-K(1)-Cl(1)#1	112.17(5)
Cl(1)#4-Ru(1)-Cl(1)#5	180.00	Cl(1)#8-K(1)-Cl(1)#1	112.17(5)
Cl(1)#1-Ru(1)-Cl(1)	89.39(5)	Cl(1)#4-K(1)-Cl(1)#9	112.17(5)
Cl(1)#2-Ru(1)-Cl(1)	90.61(5)	Cl(1)#3-K(1)-Cl(1)#9	112.17(5)
Cl(1)#3-Ru(1)-Cl(1)	180.00	Symmetry transformations used to generate equivalent atoms: #1 x-y,x-1,-z+1 #2 -x+y+2,-x+1,z #3 -x+2,-y,-z+1 #4 y+1,-x+y+1,-z+1 #5 -y+1,x-y-1,z #6 x,y,z+1 #7 -y+1,x-y-1,z-1 #8 x,y,z-1 #9 -x+y+2,-x+1,z-1	
Cl(1)#4-Ru(1)-Cl(1)	89.39(5)		
Cl(1)#5-Ru(1)-Cl(1)	90.61(5)		

Table S5. Selected bond angles (°) for **6**-**8**.

$MA_2NaRuBr_6$ (6)

∠Br-Ru-Br		**∠Br-Na-Br**	
Br(1)#1-Ru(1)-Br(1)#2	180.0	Br(1)-Na(1)-Br(1)#4	74.71(5)
Br(1)#1-Ru(1)-Br(1)	90.04(5)	Br(1)#7-Na(1)-Br(1)#8	74.71(5)
Br(1)#2-Ru(1)-Br(1)	89.96(5)	Br(1)#7-Na(1)-Br(1)#9	74.71(5)
Br(1)#1-Ru(1)-Br(1)#3	89.96(5)	Br(1)#8-Na(1)-Br(1)#9	74.71(5)
Br(1)#2-Ru(1)-Br(1)#3	90.04(5)	Br(1)-Na(1)-Br(1)#2	74.71(5)
Br(1)-Ru(1)-Br(1)#3	180.0	Br(1)#4-Na(1)-Br(1)#2	74.71(5)
Br(1)#1-Ru(1)-Br(1)#4	90.04(5)	Br(1)-Na(1)-Br(1)#7	105.29(5)
Br(1)#2-Ru(1)-Br(1)#4	89.96(5)	Br(1)#4-Na(1)-Br(1)#8	105.29(5)
Br(1)-Ru(1)-Br(1)#4	89.96(5)	Br(1)-Na(1)-Br(1)#9	105.29(5)
Br(1)#3-Ru(1)-Br(1)#4	90.04(5)	Br(1)#4-Na(1)-Br(1)#9	105.29(5)
Br(1)#1-Ru(1)-Br(1)#5	89.96(5)	Br(1)#7-Na(1)-Br(1)#2	105.29(5)
Br(1)#2-Ru(1)-Br(1)#5	90.04(5)	Br(1)#8-Na(1)-Br(1)#2	105.29(5)
Br(1)-Ru(1)-Br(1)#5	90.04(5)	Symmetry transformations used to generate equivalent atoms: #1 x-y,x-1,-z+1 #2 -x+y+2,-x+1,z #3 -x+2,-y,-z+1 #4 -y+1,x-y-1,z #5 y+1,-x+y+1,-z+1 #6 x,y,z-1 #7 y+1,-x+y+1,-z+2 #8 -x+2,-y,-z+2 #9 x-y,x-1,-z+2 #10 x,y,z+1	
Br(1)#3-Ru(1)-Br(1)#5	89.96(5)		
Br(1)#4-Ru(1)-Br(1)#5	180.0		

$MA_2AgRuBr_6$ (7)

∠Br-Ru-Br		**∠Br-Ag-Br**	
Br(1)#1-Ru(1)-Br(1)#2	89.42(7)	Br(1)-Ag(1)-Br(1)#5	75.20(7)
Br(1)#1-Ru(1)-Br(1)#3	90.58(7)	Br(1)-Ag(1)-Br(1)#3	75.20(7)
Br(1)#2-Ru(1)-Br(1)#3	180.0	Br(1)#5-Ag(1)-Br(1)#3	75.20(7)
Br(1)#1-Ru(1)-Br(1)#4	89.42(7)	Br(1)#6-Ag(1)-Br(1)#7	75.20(7)
Br(1)#2-Ru(1)-Br(1)#4	89.42(7)	Br(1)#6-Ag(1)-Br(1)#8	75.20(7)
Br(1)#3-Ru(1)-Br(1)#4	90.58(7)	Br(1)#7-Ag(1)-Br(1)#8	75.20(7)
Br(1)#1-Ru(1)-Br(1)#5	90.58(7)	Br(1)-Ag(1)-Br(1)#6	104.80(7)
Br(1)#2-Ru(1)-Br(1)#5	90.58(7)	Br(1)#6-Ag(1)-Br(1)#3	104.80(7)
Br(1)#3-Ru(1)-Br(1)#5	89.42(7)	Br(1)-Ag(1)-Br(1)#7	104.80(7)
Br(1)#4-Ru(1)-Br(1)#5	180.00	Br(1)#5-Ag(1)-Br(1)#7	104.80(7)
Br(1)#1-Ru(1)-Br(1)	180.0	Br(1)#5-Ag(1)-Br(1)#8	104.80(7)
Br(1)#2-Ru(1)-Br(1)	90.58(7)	Br(1)#3-Ag(1)-Br(1)#8	104.80(7)
Br(1)#3-Ru(1)-Br(1)	89.42(7)	Symmetry transformations used to generate equivalent atoms: #1 -x+2,-y+2,-z+1 #2 y,-x+y+1,-z+1 #3 -y+2,x-y+1,z #4 x-y+1,x,-z+1 #5 -	
Br(1)#4-Ru(1)-Br(1)	90.58(7)		
Br(1)#5-Ru(1)-Br(1)	89.42(7)		

		x+y+1,-x+2,z #6 x-y+1,x,-z #7 y,-x+y+1,-z #8 -x+2,-y+2,-z	
MA_2KRuBr_6 (8)			
∠Br-Ru-Br		**∠Br-K-Br**	
Br(1)-Ru(1)-Br(1)#1	180.00	Br(1)#7-K(1)-Br(1)#8	71.48(3)
Br(1)-Ru(1)-Br(1)#2	89.42(4)	Br(1)#5-K(1)-Br(1)#3	71.48(3)
Br(1)#1-Ru(1)-Br(1)#2	90.58(4)	Br(1)#7-K(1)-Br(1)#9	71.48(3)
Br(1)-Ru(1)-Br(1)#3	90.58(4)	Br(1)#8-K(1)-Br(1)#9	71.48(3)
Br(1)#1-Ru(1)-Br(1)#3	89.42(4)	Br(1)#5-K(1)-Br(1)	71.48(4)
Br(1)#2-Ru(1)-Br(1)#3	180.0	Br(1)#3-K(1)-Br(1)	71.48(4)
Br(1)-Ru(1)-Br(1)#4	89.42(4)	Br(1)#5-K(1)-Br(1)#8	108.52(4)
Br(1)#1-Ru(1)-Br(1)#4	90.58(4)	Br(1)#7-K(1)-Br(1)#3	108.52(3)
Br(1)#2-Ru(1)-Br(1)#4	90.58(4)	Br(1)#5-K(1)-Br(1)#9	108.52(4)
Br(1)#3-Ru(1)-Br(1)#4	89.42(4)	Br(1)#3-K(1)-Br(1)#9	108.52(4)
Br(1)-Ru(1)-Br(1)#5	90.58(4)	Br(1)#7-K(1)-Br(1)	108.52(4)
Br(1)#1-Ru(1)-Br(1)#5	89.42(4)	Br(1)#8-K(1)-Br(1)	108.52(4)
Br(1)#2-Ru(1)-Br(1)#5	89.42(4)	Symmetry transformations used to generate equivalent atoms: #1 -x+2,-y+2,-z+1 #2 y,-x+y+1,-z+1 #3 -y+2,x-y+1,z #4 x-y+1,x,-z+1 #5 -x+y+1,-x+2,z #6 x,y,z+1 #7 x-y+1,x,-z #8 y,-x+y+1,-z #9 -x+2,-y+2,-z #10 x,y,z-1	
Br(1)#3-Ru(1)-Br(1)#5	90.58(4)		
Br(1)#4-Ru(1)-Br(1)#5	180.0		

Table S6. Selected bond angles for $MA_3Ru_2Br_9$ (**9**).

∠Br-Ru-Br			
Br(3)-Ru(1)-Br(1)	176.22(11)	Br(4)#1-Ru(1)-Br(2)#2	178.96(10)
Br(3)-Ru(1)-Br(4)	88.94(7)	Br(1)-Ru(1)-Br(2)	92.65(7)
Br(1)-Ru(1)-Br(4)	88.39(7)	Br(4)-Ru(1)-Br(2)	178.96(10)
Br(3)-Ru(1)-Br(4)#1	88.94(7)	Br(4)#1-Ru(1)-Br(2)	89.82(6)
Br(1)-Ru(1)-Br(4)#1	88.39(7)	Br(2)#2-Ru(1)-Br(2)	90.10(10)
Br(4)-Ru(1)-Br(4)#1	90.24(10)	Ru(1)-Br(1)-Ru(1)#3	68.39(12)
Br(3)-Ru(1)-Br(2)#2	90.02(8)	Ru(1)-Br(2)-Ru(1)#3	67.72(9)
Br(1)-Ru(1)-Br(2)#2	92.65(7)	Symmetry transformations used to generate equivalent atoms: #1 -x+1,y,z #2 -x+1,y,-z+1/2 #3 x,y,-z+1/2	
Br(4)-Ru(1)-Br(2)#2	89.82(6)		

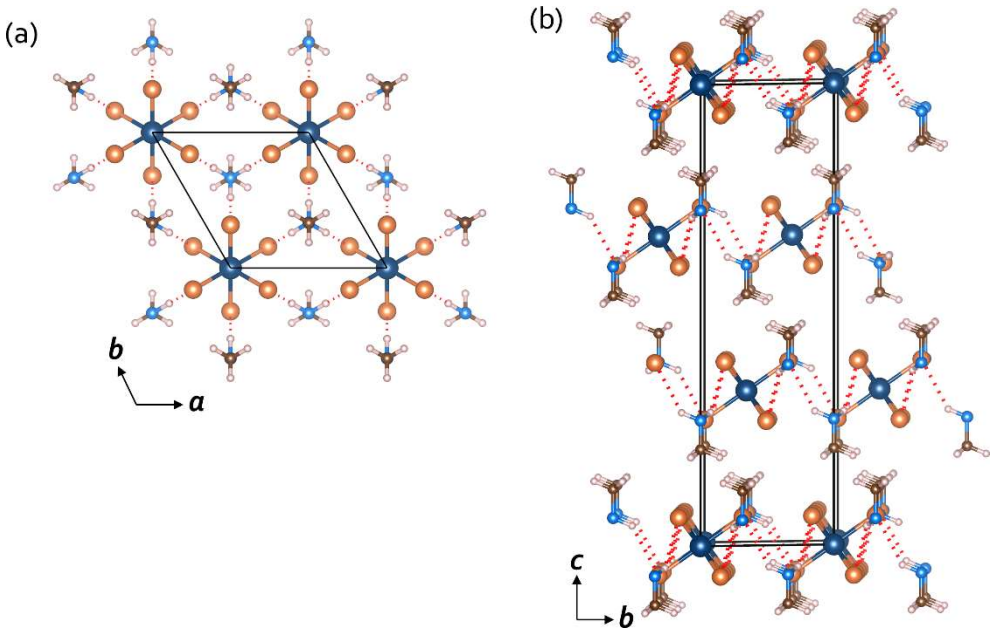

Figure S1. Hydrogen bond interactions in MA_2RuBr_6 (**2**). (a) The ball and stick model of three $RuBr_6$ octahedra connected with a methylammonium cation by hydrogen bonds. The red dotted bonds are drawn between hydrogen bond donor (N) and acceptor (Br). The packing diagram shows layer formation due to hydrogen bonds. (b) A view of layers formed in the *ab*-plane.

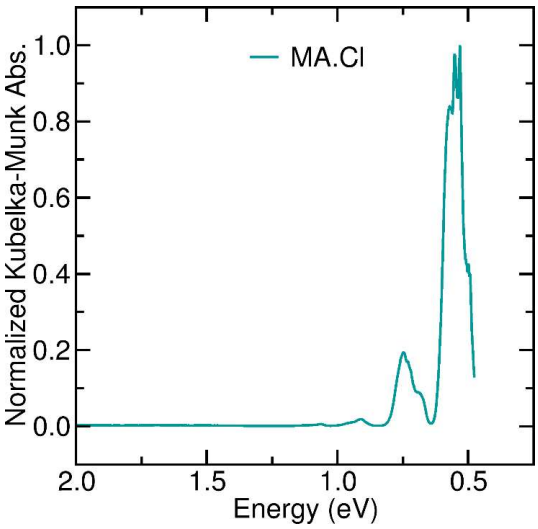

Figure S2. Kubelka-Munk spectrum of methylammonium chloride (MA·Cl).

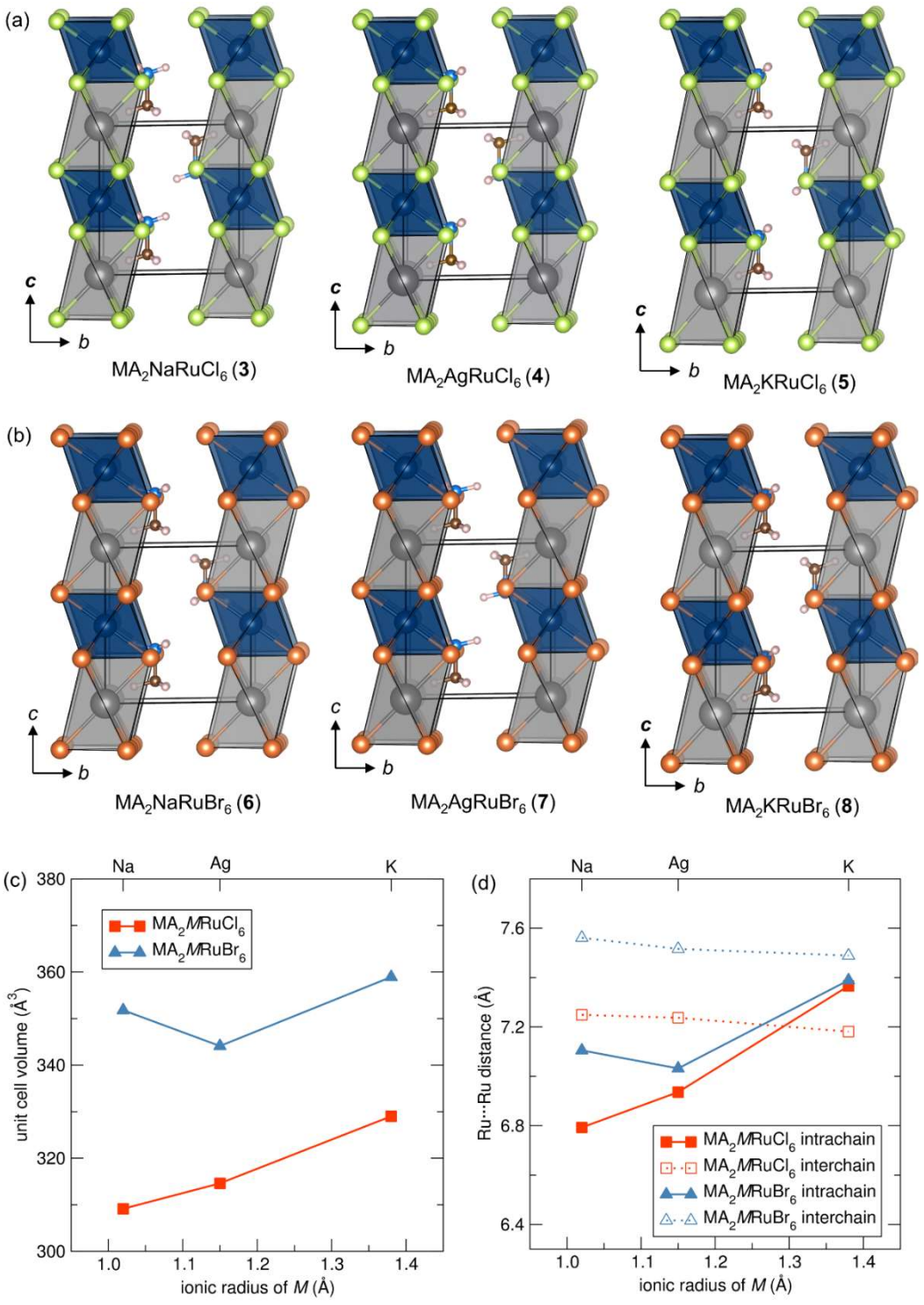

Figure S3. Single-crystal X-ray structures of MA_2MRuX_6 showing infinite chains of face-shared RuX_6 and MX_6 polyhedra. (a) MA_2MRuCl_6. (b) MA_2MRuBr_6. The structures are drawn on the same scale for the comparison of their sizes. (c) Curves showing the dependence of the unit cell volume of **3-8** on the radii of the monovalent metal ions (Na, Ag and K). (d) Curves showing the dependence of intra and interchain Ru···Ru distances on the radius of the monovalent metal ions.

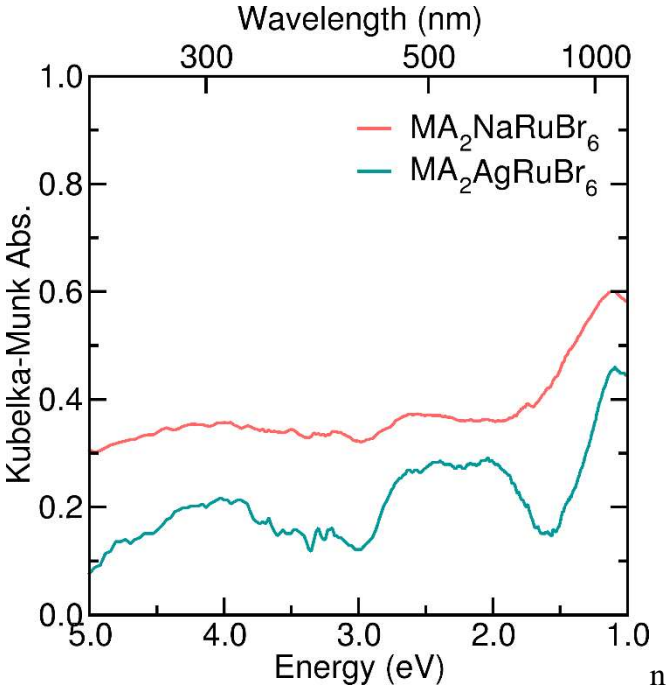

Figure S4. Kubelka-Munk spectra of $Ma_2NaRuBr_6$ (**6**) and $MA_2AgRuBr_6$ (**7**).

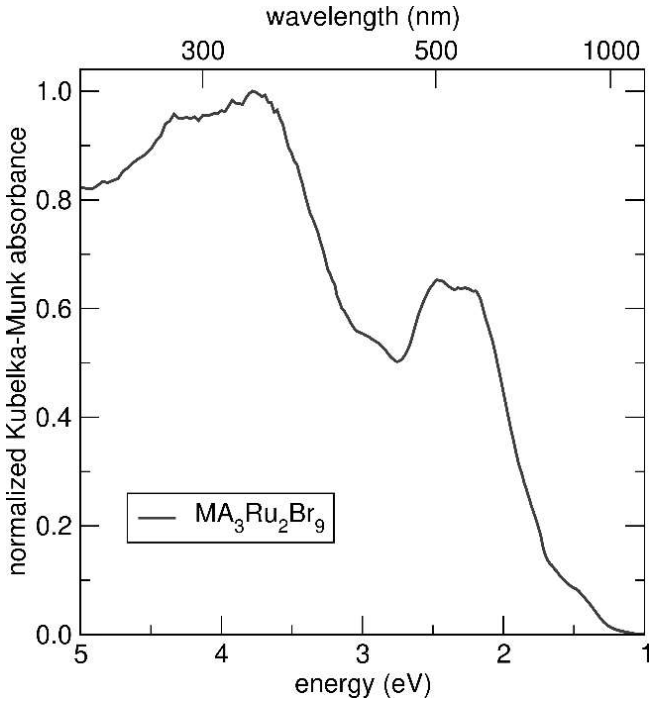

Figure S5. Absorption spectrum of $MA_3Ru_2Br_9$ (**9**).

Powder X-ray Diffraction Patterns

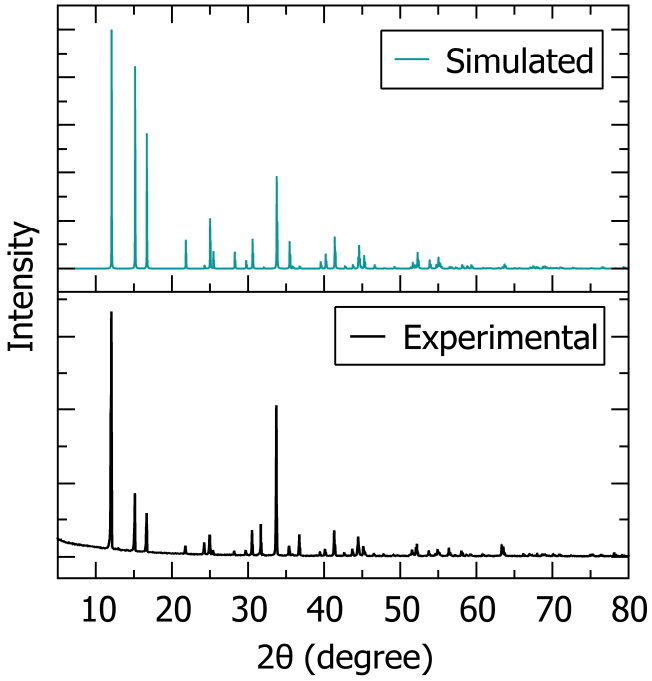

Figure S6. PXRD patterns of MA_2RuCl_6 (**1**).

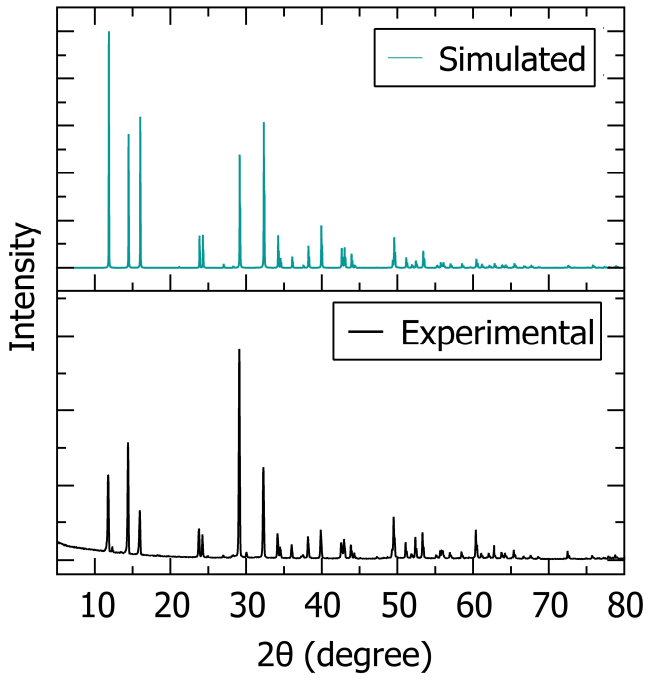

Figure S7. PXRD patterns of MA_2RuBr_6 (**2**).

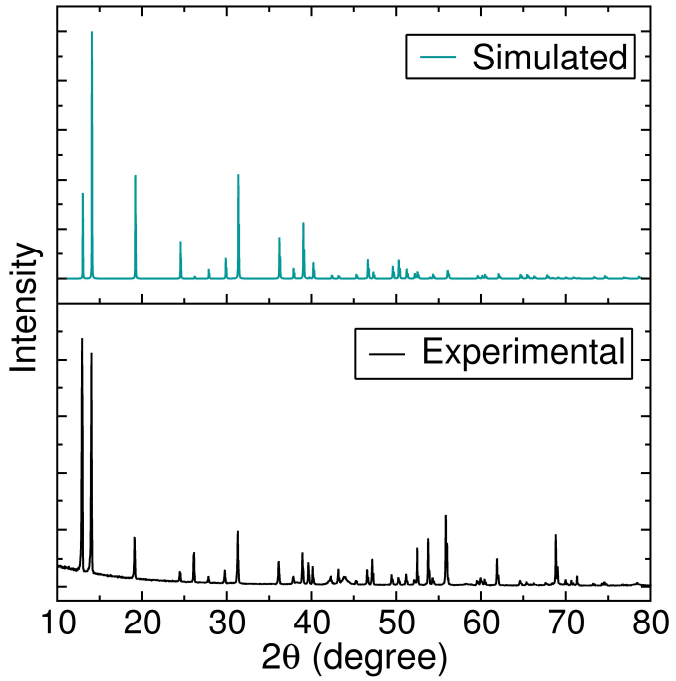

Figure S8. PXRD patterns of $MA_2NaRuCl_6$ (**3**).

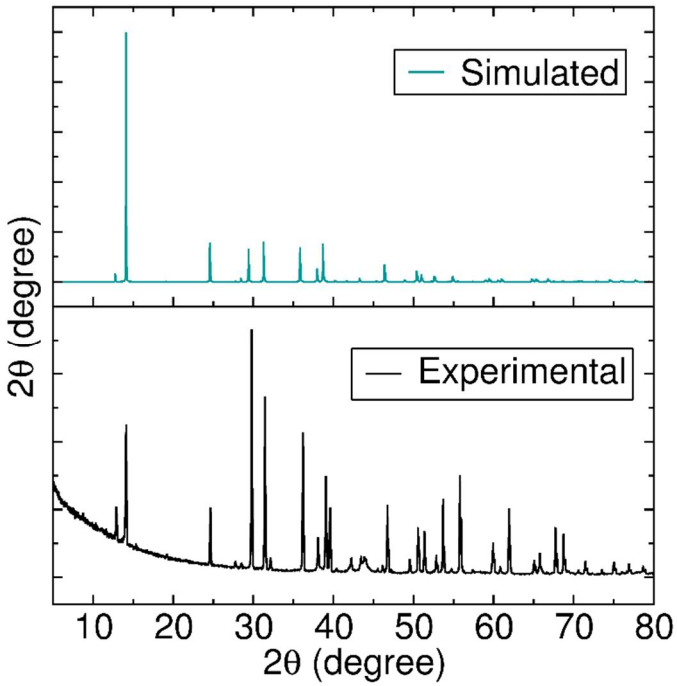

Figure S9. PXRD patterns of $MA_2AgRuCl_6$ (**4**).

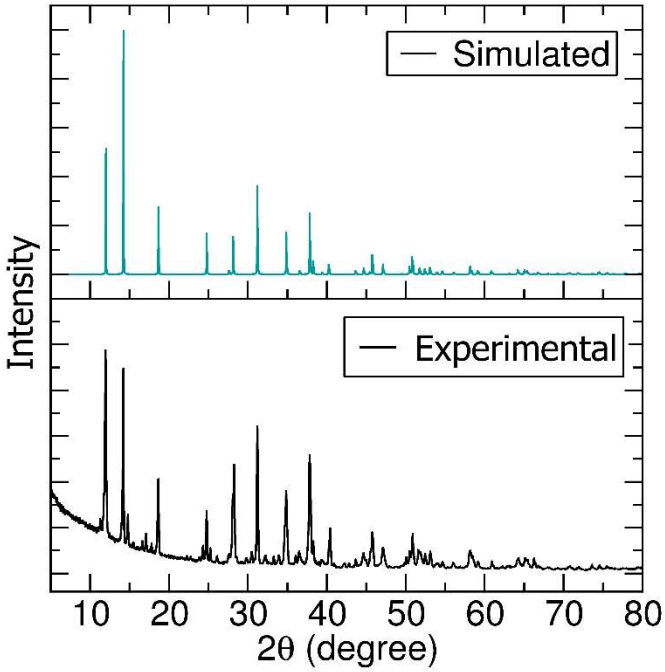

Figure S10. PXRD patterns of MA_2KRuCl_6 (**5**).

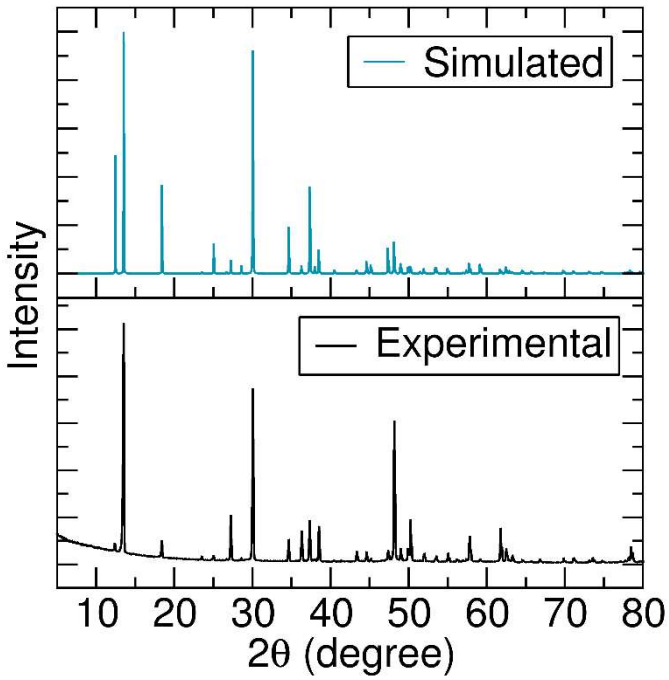

Figure S11. PXRD patterns of $MA_2NaRuBr_6$ (**6**).

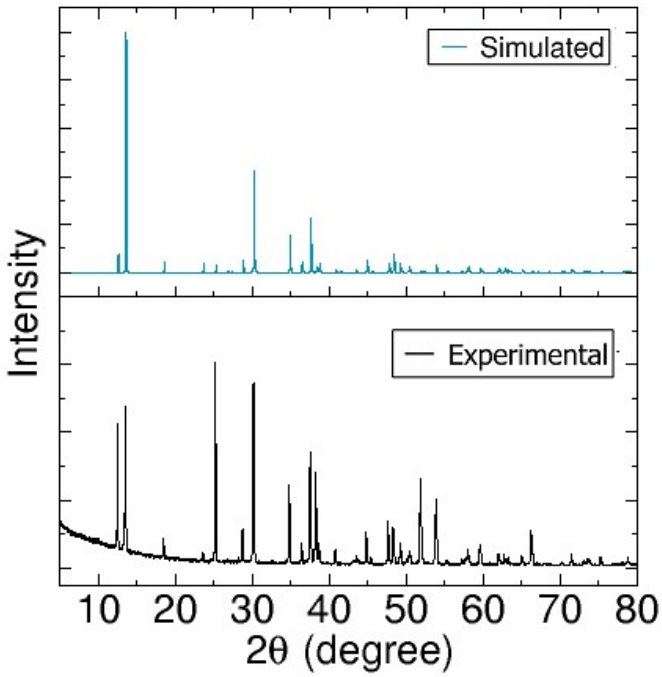

Figure S12. PXRD patterns of $MA_2AgRuBr_6$ (**7**).

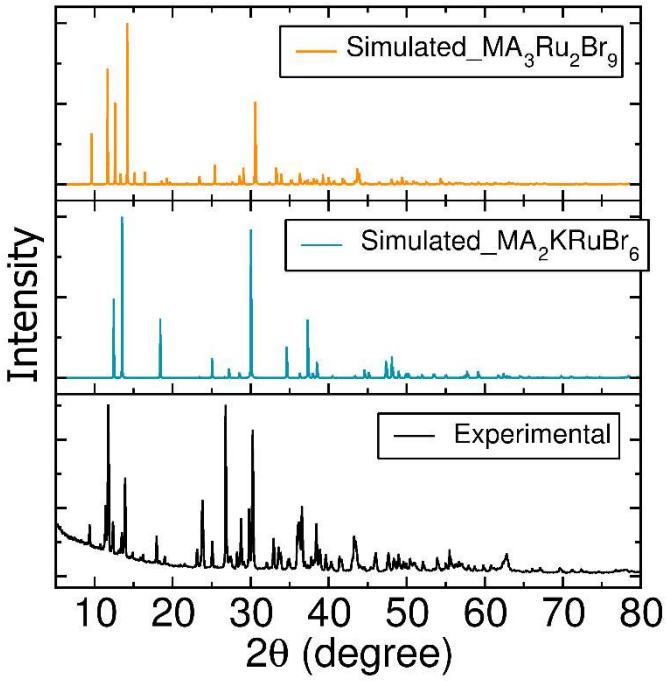

Figure S13. PXRD patterns of the mixture of MA_2KRuBr_6 (**8**) and $MA_3Ru_2Br_9$ (**9**). The peaks for both the phases can be observed in the experimental spectrum.

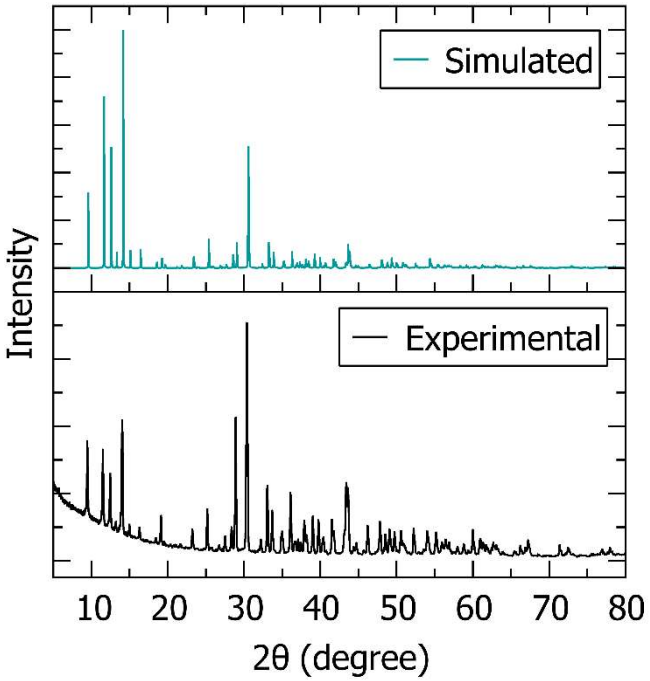

Figure S14. PXRD patterns of $MA_3Ru_2Br_9$ (**9**).

Thermal stability

The thermal stability of all these compounds has been examined by thermogravimetric analyses (TGA) (Figures S15-S22). MA_2RuCl_6 (**1**), MA_2RuBr_6 (**2**), $MA_2NaRuCl_6$ (**3**), $MA_2AgRuCl_6$ (**4**), MA_2KRuCl_6 (**5**), $MA_2NaRuBr_6$ (**6**) and $MA_2AgRuBr_6$ (**7**) begin to decompose at 248, 251, 302, 296, 260, 330 and 300 °C, respectively. The 1D compounds (**3**-**7** with the exception of **5**) are thermally more stable than the others, which is most likely due to their more condensed structures. The thermal decomposition of **8** was not carried out because it has not been obtained in the pure phase. The dimer **9** decomposes at 290 °C (Figure S22). All these compounds decompose at lower temperatures than the all-inorganic compound K_2RuCl_6 (Figure S23) which decomposes above a temperature of 450 °C. Such a trend of thermal stability has been previously observed in other double perovskites such as $MA_2AgBiBr_6$ and $Cs_2AgBiBr_6$. The $Cs_2AgBiBr_6$ phase is thermally more stable than $MA_2AgBiBr_6$.[2]

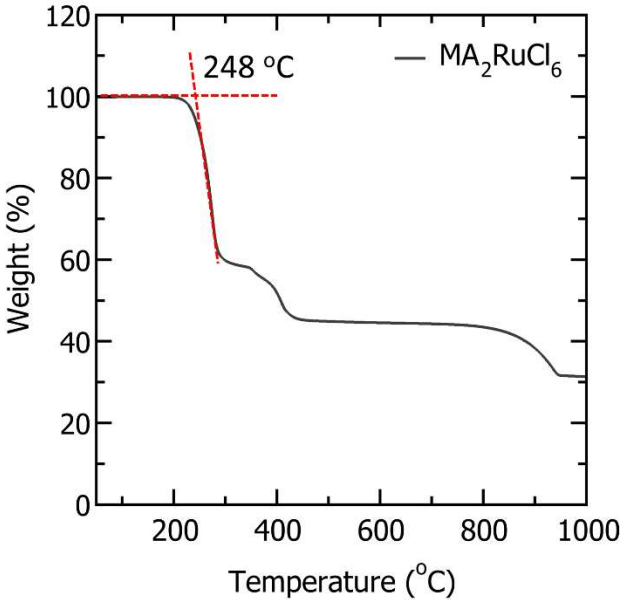

Figure S15. TGA curve of MA_2RuCl_6 (**1**).

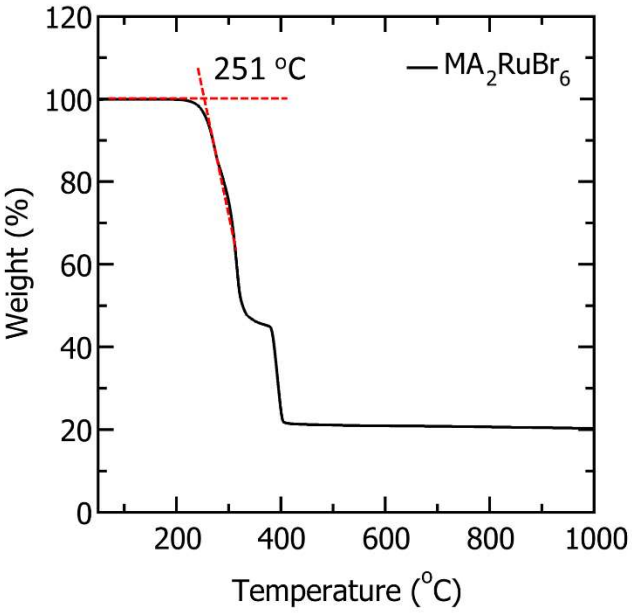

Figure S16. TGA curve of MA_2RuBr_6 (**2**).

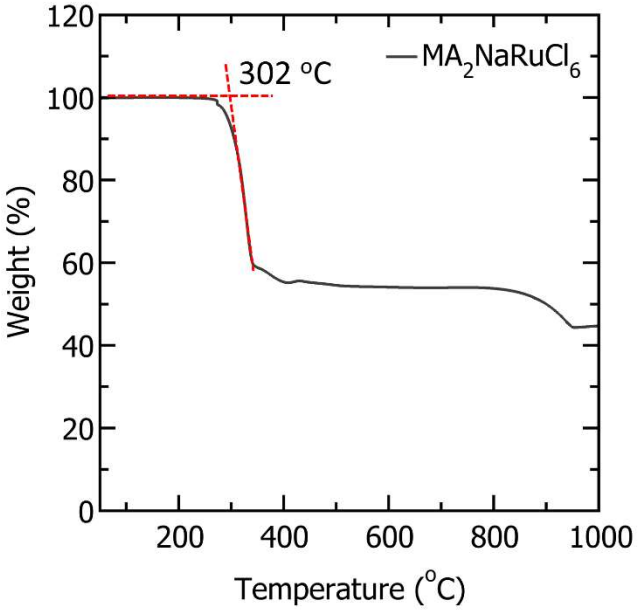

Figure S17. TGA curve of $MA_2NaRuCl_6$ (**3**).

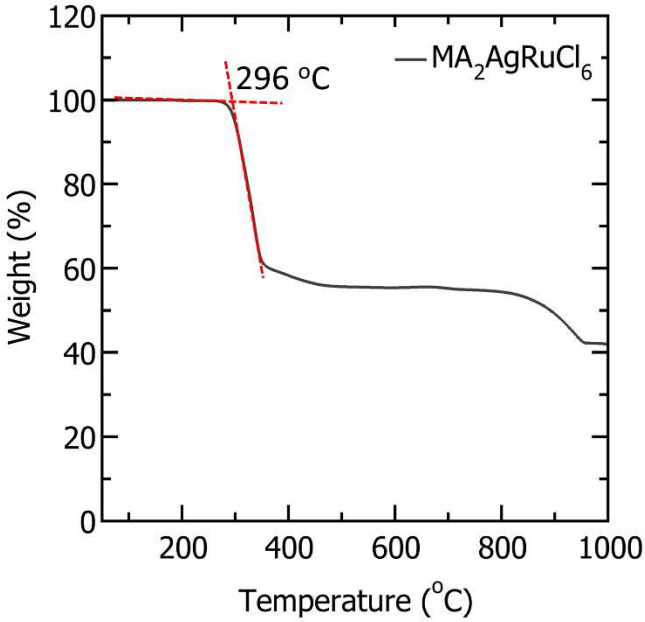

Figure S18. TGA curve of $MA_2AgRuCl_6$ (**4**).

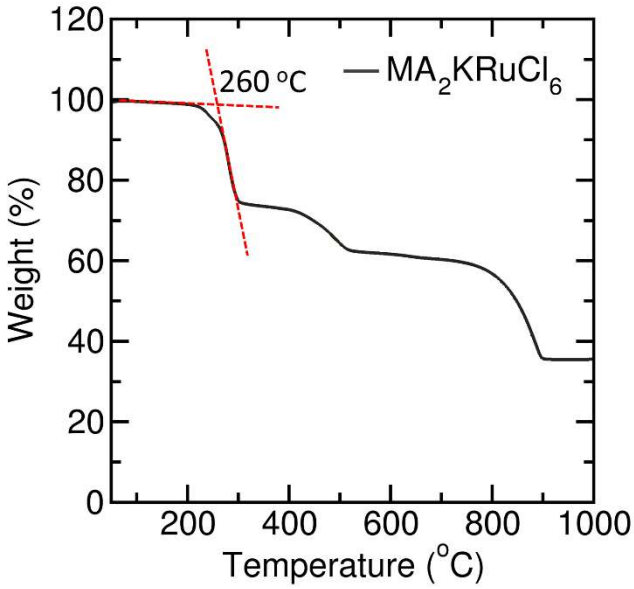

Figure S19. TGA curve of MA_2KRuCl_6 (**5**).

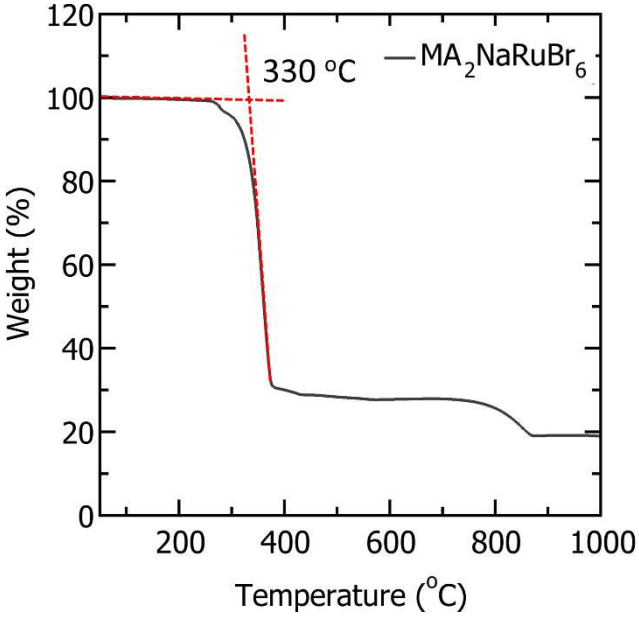

Figure S20. TGA curve of $MA_2NaRuBr_6$ (**6**).

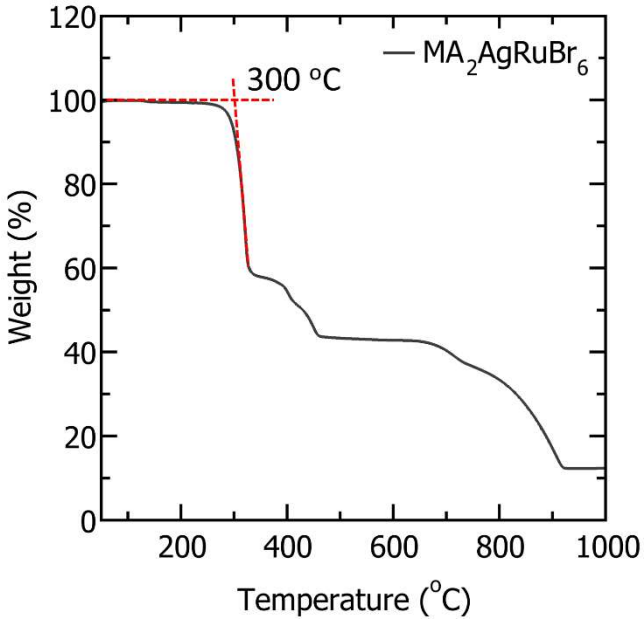

Figure S21. TGA curve of $MA_2AgRuBr_6$ (**7**).

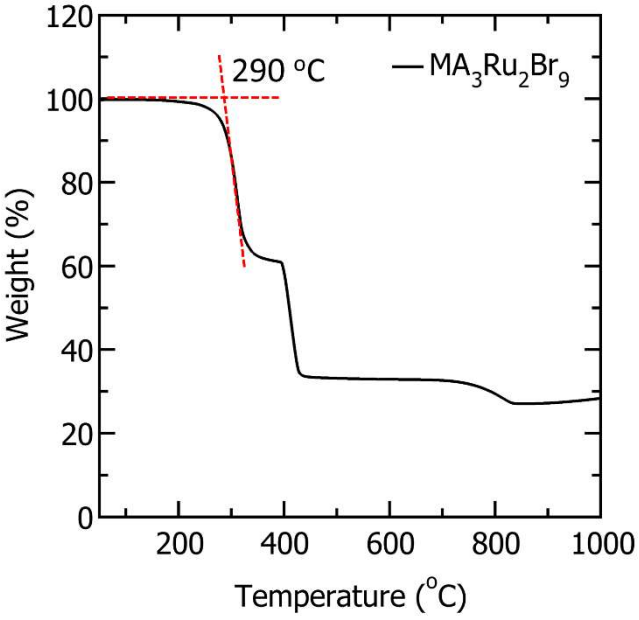

Figure S22. TGA curve of $MA_3Ru_2Br_9$ (**9**).

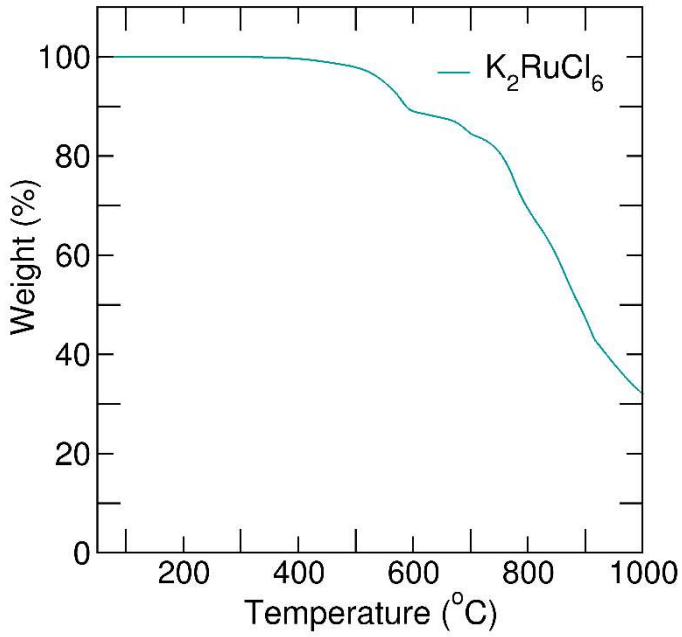

Figure S23. TGA curve of K_2RuCl_6.

Magnetic Measurements

The temperature dependence of the magnetic susceptibilities of MA_2RuCl_6, $MA_2NaRuCl_6$ and $MA_3Ru_2Br_9$ are shown in Figure S24. The susceptibilities of $MA_2NaRuCl_6$ and $MA_3Ru_2Br_9$ are largely temperature independent, while the magnetic susceptibility of MA_2RuCl_6 features a broad plateau as the thermal population of the high angular moment $J = 1$ state decreases in favor of the ground $J = 0$ state.

$MA_2NaRuCl_6$ is the only compound measured that follows Curie-Weiss behavior at high temperatures. We performed a Curie-Weiss fit between 150 to 300K (Figure S25) and find antiferromagnetic correlations of magnitude $\theta_{CW} = -14.1$K. While there are no super exchange pathways between $RuCl_6$ octahedra, the increased interactions between $RuCl_6$ octahedra is likely due to face-sharing connectivity through $NaCl_6$ polyhedra.

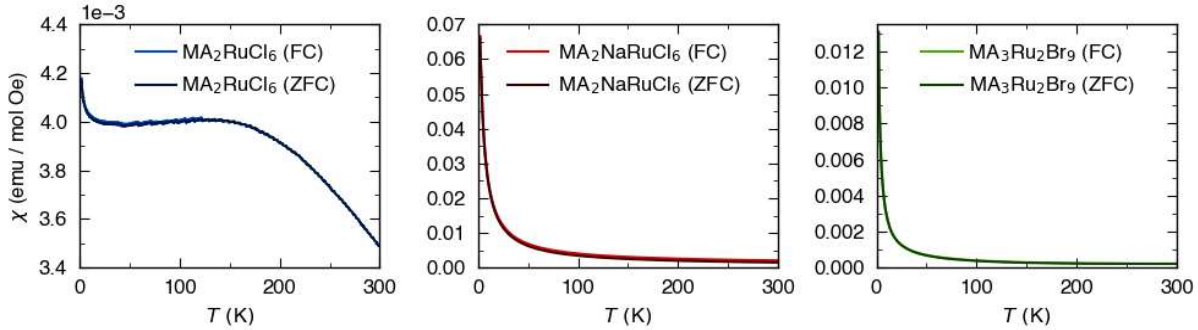

Figure S24. The magnetic susceptibilities of MA_2RuCl_6, $MA_2NaRuCl_6$, and $MA_3Ru_2Br_9$ measured between 2 to 300K under a 500Oe field on warming.

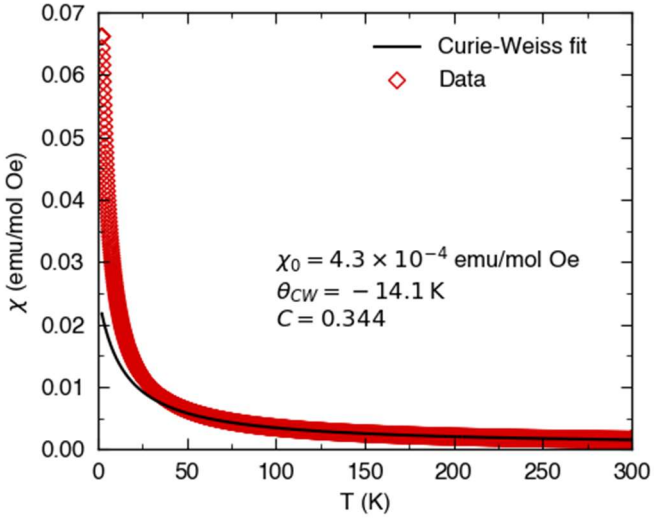

Figure S25. A Curie-Weiss fit of $MA_2NaRuCl_6$ reveals increased interactions between Ru octahedra in this compound. Antiferromagnetic interactions (θ_{CW} = -14.1K) could be responsible for the lower than expected effective magnetic moment from ideal Kotani behavior.

References

[1] G. M. Sheldrick, *Acta Crystallogr. Sect. C* **2015**, *71*, 3–8.

[2] F. Wei, Z. Deng, S. Sun, F. Zhang, D. M. Evans, G. Kieslich, S. Tominaka, M. A. Carpenter, J. Zhang, P. D. Bristowe, et al., *Chem. Mater.* **2017**, *29*, 1089–1094.